Advances in Ophthalmology Practice and Research 3 (2023) 67–79

Contents lists available at ScienceDirect

Advances in Ophthalmology Practice and Research

journal homepage: www.journals.elsevier.com/advances-in-ophthalmology-practice-and-research

Review

Advances in swept-source optical coherence tomography and optical coherence tomography angiography

Fang Zheng [a], Xiaofeng Deng [b], Qi Zhang [a], Jingliang He [a], Panpan Ye [a], Shan Liu [c], Peng Li [b], Jian Zhou [d], Xiaoyun Fang [a,*]

[a] Eye Center, The Second Affiliated Hospital Zhejiang University School of Medicine, Hangzhou, China
[b] State Key Lab of Modern Optical Instrumentation, College of Optical Science and Engineering, Zhejiang University, Hangzhou, China
[c] Department of Ophthalmology, Shanghai General Hospital, Shanghai Jiao Tong University School of Medicine, Shanghai, China
[d] TowardPi (Beijing) Medical Technology Ltd, Shanghai, China

ARTICLE INFO

Keywords:
Swept-source optical coherence tomography
Swept-source optical coherence tomography angiography
Anterior segment
Vitreous
Posterior segment

ABSTRACT

Background: The fast development of swept-source optical coherence tomography (SS-OCT) and swept-source optical coherence tomography angiography (SS-OCTA) enables both anterior and posterior imaging of the eye. These techniques have evolved from a research tool to an essential clinical imaging modality.

Main text: The longer wavelength and faster speed of SS-OCT and SS-OCTA facilitate better visualization of structure and vasculature below pigmented tissue with a larger field of view of the posterior segment and 360-degree visualization of the anterior segment. In the past 10 years, algorithms dealing with OCT and OCTA data also vastly improved the image quality and enabled the automated quantification of OCT- and OCTA-derived metrics. This technology has enriched our current understanding of healthy and diseased eyes. Even though the high cost of the systems currently limited the widespread use of SS-OCT and SS-OCTA at the first beginning, the gap between research and clinic practice got obviously shortened in the past few years.

Conclusions: SS-OCT and SS-OCTA will continue to evolve rapidly, contributing to a paradigm shift toward more widespread adoption of new imaging technology in clinical practice.

1. Introduction

Optical Coherence Tomography (OCT) was originally introduced in 1991 and has been used for in vivo imaging of retina.[1] It enables noninvasive imaging of the retina and anterior segment. It is widely used to identify and monitor pathologic changes related to different diseases such as cornea thickness, anterior chamber depth, intraretinal fluid, subretinal fluid, and exudation. From time-domain OCT (TD-OCT) with 400 A-scans per second to spectral-domain OCT (SD-OCT) with 20,000–40,000 A-scans per second, significant improvement in image resolution, the field of view (FOV), and decreased motion artifact has largely broadened the clinical acceptance and utility of OCT. The high speed of SD-OCT also enables the development of OCT angiography (OCTA) based on the difference in backscattering of light from the back of the eye on different repeated scans in the same location.[2] In 2010, Fujimoto et al. demonstrated ultrahigh speed swept-source OCT (SS-OCT) imaging using a short-cavity swept laser at 100,000–400,000 A-scans per second.[3] The high speed and the long wavelength (~1050 nm) of SS-OCT allow very high spatial resolution, even larger FOV, improved tissue penetration, and superior sensitivity roll-off performance.

This article reviews the recent development in using SS-OCT/SS-OCTA for the noninvasive assessment of different ocular structures in health and disease.

2. Principles of SS-OCT and SS-OCTA

Unlike TD-OCT, which scans axially through an optical delay line, Fourier-domain OCT (FD-OCT) records each spectral component from the interference spectrum and then performs Fourier transform on the interference spectrum to reconstruct the information in the depth direction of the sample.[4,5] According to the different detection methods, the FD-OCT can be further divided into SD-OCT and swept-source OCT (SS-OCT).[6] The main structure of SS-OCT is illustrated in Fig. 1. Unlike SD-OCT, which has a low-coherence light source and an interference spectrum obtained by spectral splitting, SS-OCT generally uses a broadband swept source whose light source wavelength varies with time. The

* Corresponding author. Eye Center, The Second Affiliated Hospital Zhejiang University School of Medicine, 01 Xihu Blvd., 310009, Hangzhou, China.
E-mail address: xiaoyunfang@zju.edu.cn (X. Fang).

https://doi.org/10.1016/j.aopr.2022.10.005
Received 4 May 2022; Received in revised form 19 October 2022; Accepted 31 October 2022
Available online 25 November 2022

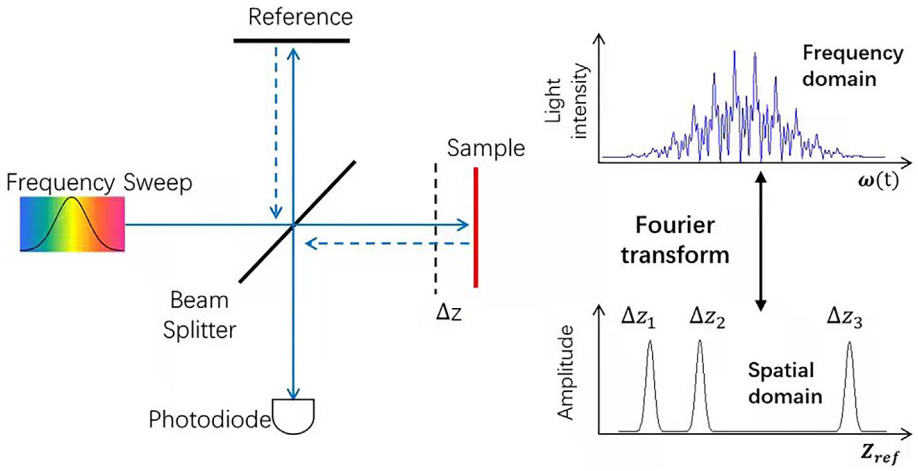

Fig. 1. The structure and data process of a typical SS-OCT system.

interference signals of the backscattered light of the sample and reference arm at different times correspond to different spectral components. A high-speed single-point detector is used to detect the interference spectrum in a time-sharing way. The reflectance distribution at different depths of the sample can be obtained by performing the Fourier transform of the interference spectrum. The procedure of time-sharing detection and Fast Fourier Transform (FFT) performed on interference spectrum is equivalent to time-modulating the wavenumber of the light source. Although additional optimization is required to maintain phase stability, SS-OCT has better sensitivity attenuation characteristics and greater scalability in imaging speed and range than SD-OCT.[3] The imaging speed of SS-OCT is mainly determined by the sweep frequency of the swept source. With the development of high-speed swept-frequency light source technology, SS-OCT can currently achieve a line scan rate of 9.4 MHz with a high signal-to-noise ratio (SNR).[7]

The SS-OCT imaging system has the advantages such as fast scanning rate, wide scanning range, narrow linewidth, and high output power. In a prototype SS-OCT system with a wavelength of 1050-nm and an A-scan rate of 400 kHz reported by Fujimoto's group, a vertical-cavity surface-emitting laser (VCSEL) light source was integrated into a commercial ophthalmic surgical microscope, enabling wide-field intraoperative viewing in the posterior and anterior eye.[8]

The advantages of SS-OCT bring benefits to OCT angiography (SS-OCTA), thus enabling noninvasive and depth-resolved imaging of the retinal and choroidal microvasculature. Compared with fluorescein angiography (FA) and other invasive imaging methods based on exogenous fluorescent dyes, the basic principle of SS-OCTA technology is the analysis of motion contrast between red blood cells (RBCs) and surrounding static tissues in blood flow.[9] The motion contrast can be explained by a random vector model, which assumes that each pixel of the OCT image is the sum of several randomly distributed scattering particles with a sub-pixel size. For dynamic blood flow regions, the spatial distribution of scattered particles exhibits time-varying characteristics due to the motion of RBCs; thus, the summed signal has a time-varying amplitude and phase; in contrast, the scattered particles in the static tissue region are relatively stable, and the summed signal does not change with time. The different time-varying characteristics of dynamic and static signals constitute the endogenous motion contrast of blood flow.

To quantify the motion contrast, OCTA technology usually requires repeated scans in the same spatial position during data collection to facilitate the analysis of signal changes over time. Up to now, several OCTA algorithms (such as variance, differential, decorrelation, and maximum likelihood estimation) have been proposed to estimate the motion magnitude of red blood cells (RBCs) utilizing different components of OCT signals (e.g., amplitude, phase, or complex).[10–12] Among them, the complex-based method contains both amplitude and phase components from OCT signals, providing superior vascular contrast and plentiful microvascular information. In addition, the decorrelation method calculates the differences between repeated tomograms, which is insusceptible to the interference caused by the overall intensity changes of the light source. Combining the above advantages, the complex-decorrelation technique provided superior vascular contrast and derived the calculation of the cross-decorrelation coefficient for complex OCT signals:

$$D(z,x) = 1 - \frac{\left|\sum_{p=0}^{P-1}\sum_{q=0}^{Q-1} A_n(z+p,x+q)A_{n+1}^{*}(z+p,x+q)\right|}{\sqrt{\sum_{p=0}^{P-1}\sum_{q=0}^{Q-1}[A_n(z+p,x+q)]^2}\sqrt{\sum_{p=0}^{P-1}\sum_{q=0}^{Q-1}[A_{n+1}(z+p,x+q)]^2}}$$

where $A_n(z,x)$ and $A_{n+1}(z,x)$ are paired complex-valued B-frames collected at the same location. n is the repeated frame index, and * means the complex conjugate. P and Q are the window sizes in the Z and X directions, respectively. p and q are the corresponding indexes of pixels within the decorrelation window.

However, the measured motion contrast is not solely dependent on the dynamics of RBCs, but is also influenced by the intensity of the scattering signal and the random noise, i.e., local SNR. Particularly, due to the normalization operation in the decorrelation calculation, random noise induces severe decorrelation artifacts and hinders the visibility of the vasculature. An intensity mask was generated with a global intensity threshold to directly exclude the regions without sufficient SNR,[13] which is much more straightforward but also excludes the possible flow signals in the low- SNR regions.

The recently proposed ID-OCTA is a promising algorithm based on a universal asymptotic linear relation between inverse SNR (iSNR) and complex decorrelation (ID) and serves as an SNR-adaptive classifier of motion contrast.[14] In this algorithm, the distribution boundary line D_c of static signals in blood flow is defined as follows:

$$D_c = \left(1 + 3\sqrt{\frac{G}{N}}\right) iSNR$$

where G is the coefficient of variance (CoV) parameter and is approximately equal to 1.5. N is the spatiotemporal kernel size in the decorrelation calculation. After excluding all signals with an iSNR value greater than the boundary line D_c, the remaining components are the endogenous OCTA signals. This algorithm removes noise decorrelation artifacts in the low SNR area caused by the normalization operation in the decorrelation calculation, thus providing clear blood vessel shapes and boundaries in the angiograms. The ID-OCTA method has been applied in

vascular morphology quantification, hemodynamics, intraoperative OCTA, and other aspects.[15–17]

The decorrelation value in SS-OCTA has a monotonous relationship with the movement rate of RBCs in the blood, which can be used to further quantify hemodynamic parameters such as flow velocity.[18] The dynamic measurement range (the slowest and fastest measurable velocity) is vital for decorrelation-based flow rate quantification. Fujimoto's group reported a variable interscan time analysis (VISTA) method, which combines measurements from different time intervals to obtain a larger velocity measurement range (compared to a single time interval).[19] However, the velocity measured using the VISTA method is relative velocity. Thus far, there has been no absolute OCTA-based velocity measurement algorithm for ocular use. Using a model-based statistical method of eigendecomposition (ED) analysis of the complex OCT signals obtained with the OCTA scanning protocol, Wang's group proposed a practical approach to statistically estimate the mean capillary flow velocity of mouse brain.[20] Even though the relationship between the mean frequency measured by the ED-based algorithm and the actual flow speed still needs to be further systematically investigated, it provides the opportunity to quantify capillary blood flow in vivo. By introducing the concepts of capillary transit time heterogeneity and capillary mean transit time, OCTA velocimetry has proved helpful in imaging microcirculatory dynamics in animal models, enabling a more comprehensive understanding of hemodynamic-metabolic coupling.[21] Combining this algorithm with SS-OCTA data will provide more information about microcirculation in various tissues of the body, including the retina.

3. SS-OCT and SS-OCTA for the anterior segment

Anterior segment SS-OCT has been used for the visualization and measurement of the tear film, conjunctiva, individual layer of the cornea, anterior chamber angle (ACA), iris, lens, horizontal extraocular muscle, and scleral[22–26] (Fig. 2). Compared with SD-OCT, the longer-wavelength light source of SS-OCT allows for high-contrast images of the entire anterior chamber until the posterior surface of the lens. It can also serve as a tool to measure the axial length (AL) of the human eye (IOLMaster 700, Carl Zeiss Meditec AG, Jena, Germany). The high speed of SS-OCT enables ultrafast acquisition of numerous longitudinal and transverse scans to create three-dimensional views, such as a 360-degree evaluation of the ACA. Using SS-OCT scans, objective measurements of inflammatory cells and aqueous flare can be achieved, providing a comprehensive assessment of anterior chamber inflammation.[27] ANTERION (Heidelberg Engineering, Heidelberg, Germany) and CASIAII (Tomey, Nagoya, Japan) are two commercially-available widely used SS-OCT systems specially designed for the anterior segment. These two instruments had built-in software for the measurement of anterior segment structures. It can be used to access clinically relevant parameters such as corneal topography, corneal topography, anterior segment analysis, biometry, and calculation of intraocular lens (IOL) power. Even though the measurements of some anterior structures obtained with different SS-OCT devices were highly repeatable and reproducible, numerical agreement is inadequate for their interchangeable use in clinical practice.[28]

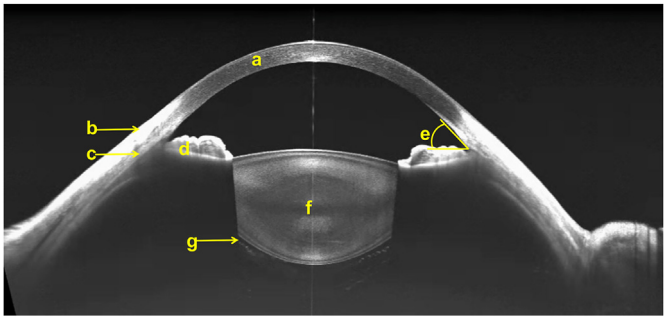

Fig. 2. A 24-mm SS-OCT B-scan (Yalkaid YG-100K, TowardPi Medical Technology, Beijing, China) showing the structure of the anterior segment, including cornea (a), conjunctive (b), sclera (c), iris (d), anterior chamber angle (e), lens (f) and Berger's space (g).

3.1. SS-OCT and cornea

SD-OCT seems sufficient for the clinical evaluation of many corneal diseases. However, SS-OCT is still able to provide more valuable information. SS-OCT can diagnose keratoconus with high accuracy.[29] Using the equation derived from SS-OCT parameters is a promising method for predicting visual function in patients with keratoconus.[30] For patients undergoing corneal transplantation or patients with Fuchs endothelial corneal dystrophy, SS-OCT provided more reliable and repeatable anterior segment evaluations when compared with the Scheimpflug system.[31,32] SS-OCT is also a sensitive tool in detecting early graft detachment after Descemet membrane endothelial keratoplasty.[33] One study showed that SS-OCT might be used as a potential non-contact device for corneal thickness assessment during laser in situ keratomileuses. However, OCT tends to underestimate stromal bed thickness (SBT) compared with ultrasound pachymetry, and these measurements may not be used interchangeably.[34] Although SS-OCT provided reproducible measurements of corneal thickness and epithelial thickness in normal eyes with a strong correlation to SD-OCT, both technologies are not interchangeable when the main thickness parameters are used to diagnose early keratoconus or calculate the expected residual SBT before corneal refractive surgery.[35]

3.2. SS-OCT and lens

Some SS-OCT devices provide the visualization of the whole crystalline lens, showing utility for in vivo imaging of lens sutures, age-related changes of the lens, cataract quantification, and density documentation.[36–38] Lens measurements using this technology have been shown to be highly reproducible.[39] The SS-OCT enables whole-eye length imaging and high-precision, non-contact ocular biometry to calculate IOL power. The correlations between crystalline lens tilt and IOL tilt using whole-eye scanning indicate that preoperative tilt determination using SS-OCT could help predict postoperative IOL tilt, assist in IOL (toric) power calculations, and potentially improve visual outcomes.[40] An SS-OCT study showed that the magnitude of crystalline lens tilt decreased with increasing AL. While the variability in the tilt orientation increased with increasing AL, the direction of tilt was predominantly toward the upper outer quadrant in both eyes.[41] Excellent agreement was established between the measurements provided by the new optical biometer based on SS-OCT and the optical biometer using Scheimpflug imaging.[42] Higher AL values were measured by SS-OCT than ultrasound.[43]

3.3. SS-OCT and anterior chamber angle

Imaging the ocular anterior chamber with SS-OCT has further enhanced our understanding of the risk factors and mechanisms involved in angle-closure diseases. The higher scan speed and deeper tissue penetration ability of SS-OCT enable imaging of the entire anterior chamber in one frame. Moreover, the qualitative and quantitative assessment of the ACA, iris, and lens can be accomplished with a single scan.[44–46] The three-dimensional and 360-degree analysis feature of SS-OCT enables quantification of the amount of circumferential iridotrabecular contact (ITC), which has the potential to provide objective information about the extent of circumferential angle closure.[47,48]

Apart from the established risk factors for angle closure, such as shallower anterior chamber depth, shorter AL, thicker and anteriorly placed lens, female sex, and older age,[49,50] several novel SS-OCT imaging biomarkers have been identified as risk factors for developing angle closure, including smaller anterior chamber width, area, and volume, thicker iris with greater curvature, and increased lens vault.[51–53] The

overall diagnostic performance of SS-OCT in detecting gonioscopic-defined angle closure was better than that reported for TD-OCT. The semiautomatic assessment of ITC from SS-OCT images is time-saving, with a similar diagnostic performance as the manual assessment.[48] Interestingly, SS-OCT tends to classify more angle closure than gonioscopy.[47,54,55] More disagreement between these two modalities was seen when the anterior chamber depth was around 2.4 mm.[56] Baskaran et al. found that angle closure on SS-OCT at baseline tended to develop more gonioscopic angle closures at four years. It is, therefore, important for clinicians to consider close monitoring of patients with evidence of angle closure on SS-OCT, even if the angles appear open on gonioscopy.[57]

Peripheral anterior synechia (PAS) represents the anterior adhesion between the peripheral iris and the anterior chamber angle, traditionally determined by indentation gonioscopy. The multiple high-resolution, cross-sectional images of the angle can be captured within seconds, facilitating the examination and measurement of PAS.[58–60] Based on SS-OCT findings, researchers have demonstrated that phacoemulsification (PE) plus goniosynechialysis surgery resulted in a more significant reduction of ITC and the extent of PAS than PE alone in eyes with primary angle closure glaucoma and cataract.[61]

3.4. SS-OCTA and anterior segment

OCTA has been used to image pterygium, conjunctiva vessels, ocular surface tumors, normal iris vasculature, and iris neovascularization.[62,63] Most reported works in the literature were performed with SD-OCTA. The high cost of SS-OCTA has limited widespread commercial and clinical acceptance of this method in anterior segments to date. The main application of the SS-OCTA system for anterior segments is imaging the iris. Compared with SD-OCTA, the longer wavelength of SS-OCTA provides superior visualization of thicker tissue and better delineates iris vessels in normally pigmented irides.[64] SS-OCTA was used to diagnose and follow iris cysts. Iris cysts did not have intrinsic vascularity on the SS-OCTA images. It has been shown that pigment epithelial cysts generally remain stable without treatment. However, iris stromal cysts frequently require surgical intervention.[65] SS-OCTA can successfully image vasculature within moderately pigmented and non-pigmented iris melanocytic tumors.[63] Using SS-OCTA, Mastropasqua's group showed a uniform reduction in the iris vessel network one month after scleral buckle surgery, supporting the clinical use of SS-OCTA to identify early iris perfusion changes as potential predictive biomarkers of vascular disorders.[66]

4. SS-OCT for vitreous

As mentioned before, SS-OCT has enabled a more extensive imaging range and lower sensitivity roll-off than SD-OCT.[3] It provided better views of vitreous structures such as posterior precortical vitreous pockets (PPVPs), Cloquet's canal, posterior cortical vitreous, posterior hyaloid, and vitreous opacities of healthy eyes and eyes with different etiologies[67] (Fig. 3).

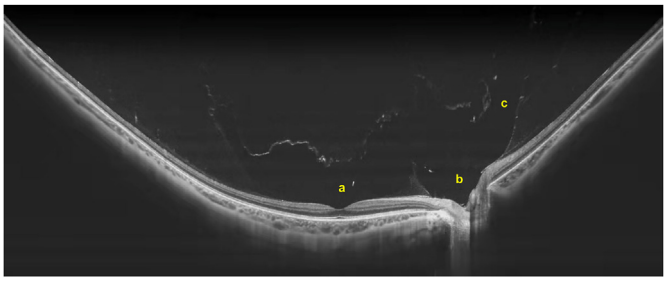

Fig. 3. A 24-mm SS-OCT B-scan (BM-400K BMizar, TowardPi Medical Technology, Beijing, China) of the right eye of a 23-year-old emmetropic female showing PPVP (a), Martegiani cavity (b), and Cloquet's canal (c) of the vitreous.

In 2013, SS-OCT with a 12-mm scan length visualized the entire structure of the PPVP for the first time.[68] Later, using a prototype SS-OCT, the normal vitreous architecture with widefield 3D-OCT was imaged.[67] In this study, researchers found that compared to high-dynamic-range and standard OCT logarithmic scale display, the vitreous window display provides the highest sensitivity for posterior vitreous and vitreoretinal interface analysis. By imaging the vitreous of children aged between 3 and 11 years using SS-OCT, Li et al. showed that PPVPs could be noticed as early as three years old. With aging, they gradually enlarged and evolved into small boat-shaped spaces, as seen in adults. The channels connecting the PPVPs and Cloque's canal began to form after age five.[69] Another SS-OCT study using en face analysis to visualize the posterior vitreous also confirmed that PPVPs and Cloquet's canal are not connected in younger patients but in older patients.[70] Compared with normal eyes, eyes with high myopia may have larger PPVPs.[71]

Historically, most observations of posterior vitreous detachment (PVD) were made using by biomicroscopy and ultrasound. Compared to these two conventional imaging modalities, SS-OCT may be a more sensitive modality for detecting PVD in patients with clear media.[72] The detection of PVD using OCT has been limited to the macular region. The development of SS-OCT enables the visualization of PVD beyond the macular. Moreover, in a study comparing 6 mm and 16.5 mm OCT images in the same eye, seven eyes were categorized as having no PVD on 6 mm OCT. However, these were upgraded to partial PVD on 16.5 mm OCT,[73] meaning that longer scans are needed for fully evaluating PVD. A study using 25-mm to 36-mm SS-OCT images montaged from three SS-OCT images demonstrated that PVD first appeared in the third decade of life.[74] Another study found that partial PVD may occur as early as five years old.[75] Compared with the normal population, people with high myopia develop partial PVD around the macula and complete PVDs at younger ages.[71] In eyes without fundus diseases, more than 40% of eyes at their PVD initiation are associated with vitreoschisis. As for location, PVD is first noted primarily in the paramacular-peripheral region and ultimately extends to fovea.[74] A newer SS-OCT device can obtain up to 23-mm of widefield B-scan images in a single acquisition. Using this widefield SS-OCT to quantitatively evaluate the PVD stage in healthy subjects, researchers found that age was significantly positively correlated with the overall PVD stage.[76] Furthermore, the PVD stages of the bilateral eyes were highly consistent in 183 subjects (85.5%). Moreover, PVD progression occurs significantly faster in female eyes than in male eyes at 60 years of age or older, suggesting that the macular pathologic features associated with PVD occur younger in women.

5. SS-OCT and SS-OCTA for the posterior segment

The most common application of SS-OCT and SS-OCTA is imaging the posterior segment and retinal-choroidal diseases, including diabetic retinopathy (DR), retinal artery/vein occlusion (ROV/RAO), age-related macular degeneration (AMD), polypoidal choroidal vasculopathy (PCV), central serous chorioretinopathy (CSCR), macular telangiectasia type 2 (MacTel2), myopia, uveitis, and others. They provide detailed qualitative and quantitative information on structure and vasculature, which is valuable for diagnosing and monitoring diseases.

5.1. Normal retina and retinal vasculature

A normal database of retinal thickness measurement using SS-OCT was been established and was different from the SD-OCT devices for the same subject.[77,78] Clinicians should be careful when comparing retinal structural measurements across different OCT devices. With SS-OCT, the retinal thickness map or en face analysis of the retina structure was no longer limited to the macula. The development of SS-OCTA has been beneficial for understanding normal retinal vasculature in a way that has not been possible before.

SS-OCTA enables retinal vasculature visualization beyond the

macula. To date, the largest FOV obtained with a single capture is 24 × 20 mm (Fig. 4). Wide-field SS-OCTA improved clinical applications for the retina. The reproducibility and repeatability for measuring certain microvasculature features using wide-field SS-OCTA are excellent in normal eyes and can be used to quantify microvascular changes over time.[79] High interocular correlation in the fovea avascular zone (FAZ) area and perimeter, moderate correlation in fractal dimension and vessel diameter index, and poor correlation in vessel density were observed in normal healthy subjects.[80] Normative data of SS-OCTA for retinal vasculature densities (VDs) and the FAZ area are not as many as SD-OCTA. To the best of our knowledge, the largest SS-OCTA normative database of retinal microvasculature was generated from 346 healthy subjects.[81] In healthy eyes, the macular VD presented with a wide range of variations, which is positively correlated with foveal retina thickness and choroidal thickness (CT), but negatively correlated with age and no correlation with AL or sex. These findings were confirmed by a similar study.[82] In contrast, one study reported that AL was negatively correlated with superficial parafoveal VD after correction for magnification induced by eye elongation.[83] Central retinal thickness and retinal VD were found to be negatively associated with FAZ.[84] Still, more researches needs to be done to investigate the repeatability of wide-field SS-OCTA in diseased eyes.

5.2. Normal choroid

The longer wavelengths of SS-OCT and SS-OCTA enable better penetration into the choroid, a breakthrough for understanding the choroid metrics of healthy and diseased eyes. Compared with being able to visualize 93% of scleral-choroidal junctions using enhanced depth imaging (EDI) SD-OCT,[85] SS-OCT allowed 100% clear visualization of the scleral-choroidal junction.[86] Therefore, the reproducibility and repeatability of CT measurements using SS-OCT are excellent.[87] The higher imaging speed of SS-OCT enables a larger FOV and denser A-scan, which makes wide-field CT maps possible. Many commercially available SS-OCT devices have built-in software to automatically generate CT maps (Fig. 5). Even though considerable variation was seen on CT maps of normal eyes, the thickest choroidal was most often located in the superior-temporal hemifields.[88] Interestingly, mean CT measurements in the right eyes were significantly thicker than in the left eyes in a healthy population.[89] A normal 95% limits of signed interocular differences and absolute interocular differences in mean CT were established, which could be used as a reference for physiological asymmetry. Besides CT, many other interesting features of the choroid were investigated using SS-OCT or OCTA, including but not limited to choroidal vessel volume (CVV), choroidal stroma volume (CSV), choroid vascularity index (CVI), and the choroidal stroma-to-vessel volume ratio (CSVR). By using a fully automated SS-OCT algorithm, Wang's group found that CT, CVV, and CSV decrease with age, and the CVI and CSVR remain constant with age.[90] The development of powerful algorithms will largely facilitate future studies into the choroid change in both ocular and systemic diseases.

SS-OCTA provided high-quality choriocapillaris (CC) images.[91,92] In these images, white pixels represent flow and black pixels represent areas of signal deficits where the flow is either absent or below the detection threshold, called “CC flow voids” and recently renamed as “CC signal voids”. By studying 164 healthy subjects with normal eyes ranging in age from 20s to 80s using SS-OCTA, Zheng et al. found that the flow deficits (FDs) increased with age across the central 5 mm of the macula in normal people, and the greatest increase was found in the central 1 mm region of the macula.[93] The correlation of FDs with distance from the fovea and age has been confirmed by many other studies.[94,95] Even though CC imaged by commercially available SS-OCTA instruments has been accepted by many researchers, it still cannot provide images that can resemble histology and resolve individual capillaries under the posterior pole. The reason is that current commercial SS-OCTA systems only have 15- to 25-μm transverse resolution, which is similar to the averaged intercapillary distance of CC (10–25 μm). Encouragingly, by introducing a prototype research SS-OCT system with a large beam size of 3.50 mm, Wang's group successfully demonstrated a clearer CC lobular capillary network.[96] The authors also point out that a small beam size could provide comparable quantification results for both morphometric parameters and CC inter-vascular spacing, indicating that the current commercial OCTA systems might still be applicable to providing useful information relevant to clinical measurements.

5.3. SS-OCT and SS-OCTA for DR

The advance of SS-OCTA provides a much larger scan area with a single scan (12 × 12mm and 24 × 20mm) or montage technique (15 × 15mm, 18 × 18mm, and 31 × 27mm). Wide-field SS-OCTA is able to capture all clinically relevant features of DR, including microaneurysms (MAs), non-perfusion areas (NPAs), intraretinal microvascular abnormalities (IRMAs), and neovascularization (NV) (Fig. 6). It also gives simultaneous OCT B-scans to detect diabetic macular edema. As the pathologic features of DR, such as NPA and NV, are often outside of the macula, wide-field SS-OCTA is particularly important for the diagnosis and management of DR.[97] The noninvasive feature of SS-OCTA enables longitudinal imaging of NV to monitor NV progression or regression.[98] The first definitive demonstration of IRMAs evolving into NV was recorded using longitudinal wide-field SS-OCTA.[99] Most importantly, the detection rate of IRMAs and NV was superior to the ultrawide-field color

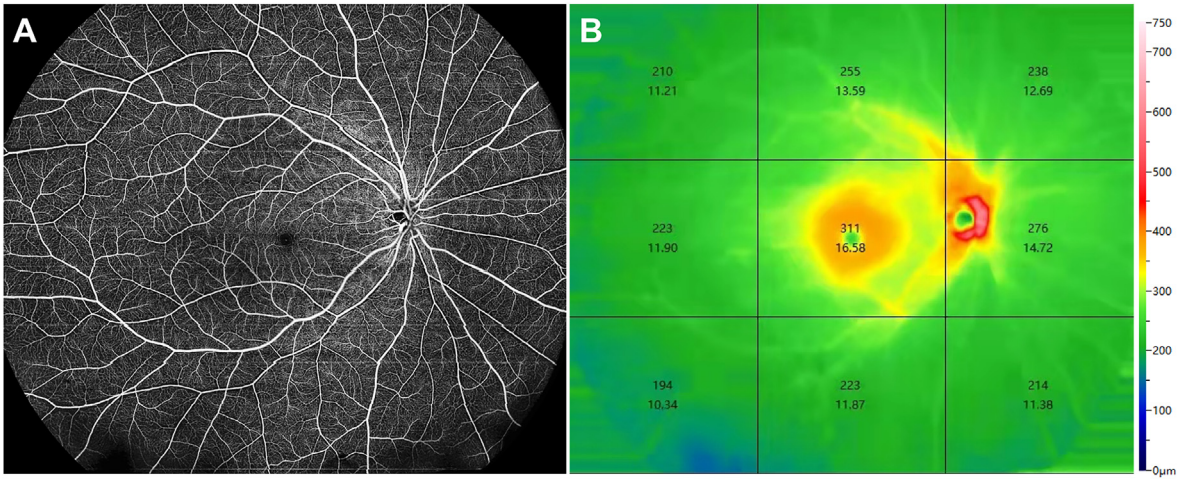

Fig. 4. Retina vessels (A) and retina thickness map (B) of the right eye of a 35-year-old emmetropic male using 24 × 20mm wide-field SS-OCTA (BM-400K BMizar, TowardPi Medical Technology, Beijing, China).

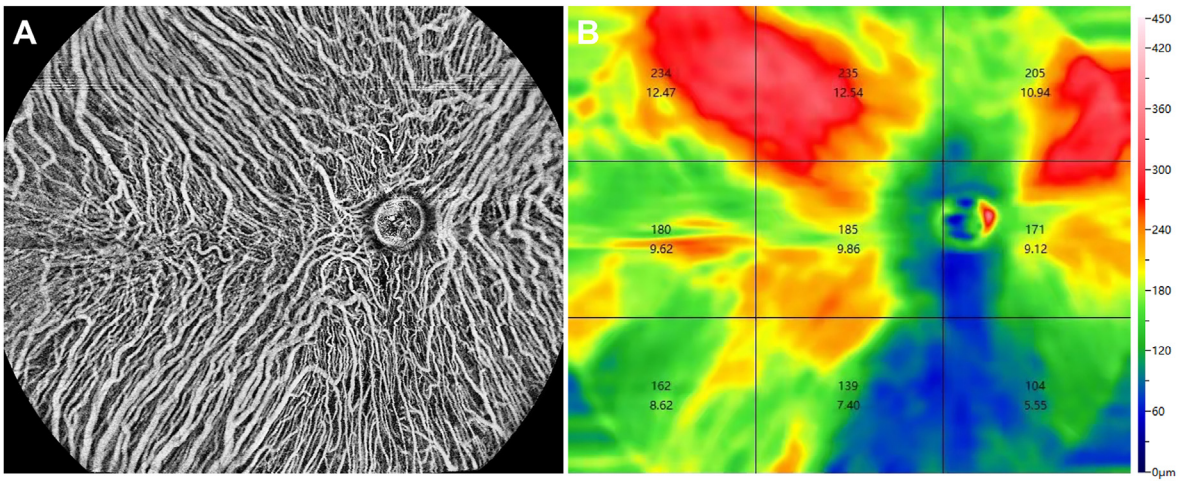

Fig. 5. Choroidal vessels (A) and choroidal thickness map (B) of the right eye of the same normal subject as Fig. 4 using 24 × 20mm wide-field SS-OCTA (BM-400K BMizar, TowardPi Medical Technology, Beijing, China).

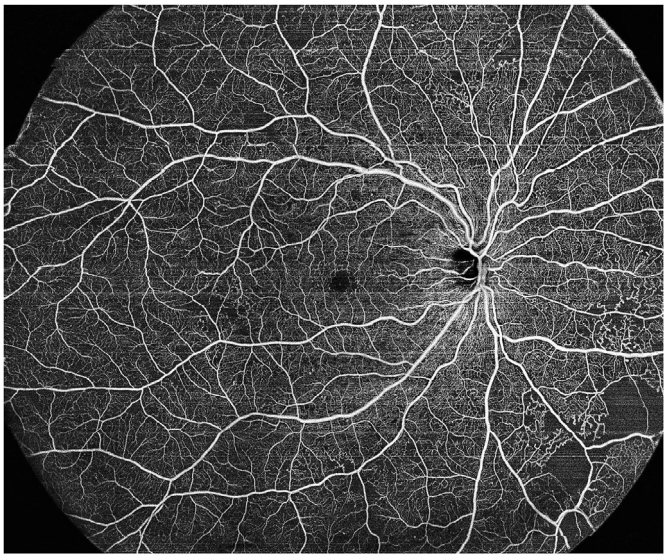

Fig. 6. The superficial vascular complex slab of the right eye of a non-proliferative diabetic retinopathy patient using wide-field SS-OCTA (BM-400K BMizar, TowardPi Medical Technology, Beijing, China).

fundus and comparable with ultrawide-field FA (UWF-FA).[100] The detection rate of NPAs was higher with wide-field SS-OCTA than with UWF-FA in eyes with DR after three anti-vascular endothelial growth factor (VEGF) injections.[101] Even though some previous studies showed lower sensitivity of SS-OCTA in the detection of MAs than FA,[102,103] a recent study suggested that the detection rates of MAs were comparable with UWF-FA images.[100] Furthermore, when comparing wide-field SS-OCTA plus UWF color fundus photograph with UWF-FA, the detection rates of MAs, IRMAs, NV, and NPAs were identical. There was a strong agreement between SS-OCTA and FA in evaluating the size of the FAZ. Progression of the FAZ size of both superficial and deep capillary plexus correlated with the DR stage.[104,105] Wide-field SS-OCTA also provides additional information about the relationship of NV with the vitreous and can be used to monitor the changes in traction before and after vitrectomy. The presence of extensive and protruded NV was associated with vitreous hemorrhage in patients with PDR.[106] A separate group demonstrated the ability of wide-field SS-OCTA imaging to characterize vitreoretinal traction, retinal ischemia, and NV-hyaloid relationships in diabetic traction retinal detachment and to monitor changes in these parameters before and after pars plana vitrectomy.[107]

Using VISTA, relative flow speed in the microvascular changes of different stages of DR was analyzed.[108] In general, increased disease severity was associated with a globally slower flow speed, particularly in the area around the FAZ. MAs, IRMAs, and NV appeared to originate from areas of relatively slow blood flow speed. MAs showed slower flow, IRMAs showed turbulent, intermediate to slow flow, and venous beading and looping presented relatively high flow speed that tapered progressively. A relatively slower flow speed was found in NV with a venous origin, whereas a relatively faster flow speed was found in NV with an arterial origin.

5.4. SS-OCT and SS-OCTA for RAO and RVO

FA is still the gold standard for evaluating RAO. Few studies on the applications of SS-OCTA in RAO have been reported. The main application of SS-OCT and SS-OCTA in retinal vascular occlusion is on RVO (Fig. 7), which is the second-most common retinal vascular disorder after DR.[109]

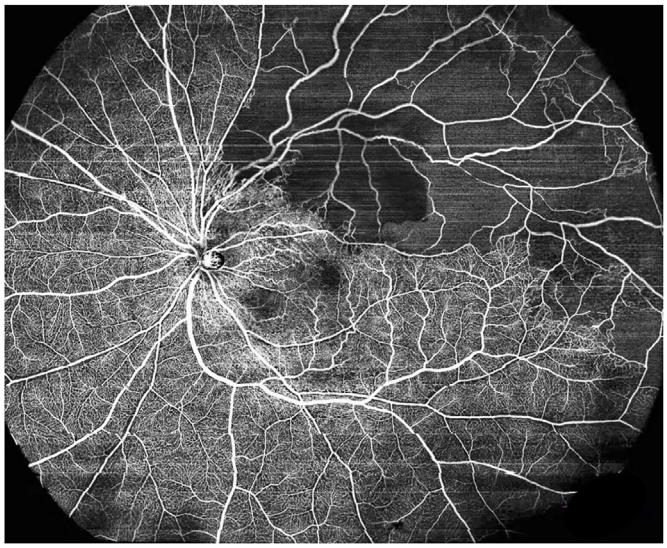

Fig. 7. The superficial vascular complex slab of the left eye of a branch retinal vein occlusion patient using 24 × 20mm wide-field SS-OCTA (BM-400K BMizar, TowardPi Medical Technology, Beijing, China).

In patients with branching RVO (BRVO), a correlation was found between NPAs on FA and honeycomb-like structure on en face SS-OCT due to retinal edema was found.[110] The dark area on the en face SS-OCT corresponding to retinal thinning can be used to delineate NPAs.[111] Increased macular thickness, disrupted retinal outer layers, and disorganization of retinal inner layers seen on SS-OCT are significant predictors of poor visual outcomes.[112] With greater accuracy, SS-OCTA was used to evaluate the perfusion status of retinal vessels qualitatively and quantitatively. A case report of BRVO demonstrated that SS-OCTA was superior to FA in detecting NPAs and delineating them with higher resolution and in detecting microvascular abnormalities and FAZ area.[113] Most conventional SS-OCT or SS-OCTA with 12 × 12mm FOV cannot be used to evaluate peripheral retinal abnormalities, such as NPAs and neovascularization of RVO. The newer wide-field SS-OCTA devices overcome this shortcoming and can be used to evaluate RVO with peripheral retinal abnormalities with comparable accuracy compared with FA.[114,115] It can be used to differentiate between ischemic and non-ischemic RVO.[116]

5.5. SS-OCT and SS-OCTA for AMD

SS-OCT and SS-OCTA provide sufficient information for monitoring both nonexudative and exudative AMD. Large and soft drusen are distinguishing features of AMD. The algorithm based on SS-OCTA for the quantitative assessment of drusen area and volume measurement was validated against the SD-OCT algorithm and was shown to be highly reproducible.[117] Wide-field en face SS-OCT images covering arcades were able to identify reticular peseudodrusen (RPD) as good as conventional multimodal imaging, including color fundus photographs, fundus infra-red images, and fundus autofluorescence.[118] En face SS-OCT imaging is also useful for detecting and monitoring of calcified drusen.[119] Using a slab located beneath the retinal pigment epithelium (RPE), geographic atrophy (GA) (also known as complete retinal pigment epithelium and outer retinal atrophy, cRORA[120]), and nascent GA (also known as incomplete retinal pigment epithelium and outer retinal atrophy, iRORA[121]) can be well visualized and measured. Compared with intact RPE, the area where RPE is attenuated or absent appears bright on the sub-RPE slab with segmentation boundaries positioned 64 and 400 μm below Bruch's membrane.[122] Using en face SS-OCT, Rosenfeld's group found that persistent hypertransmission defects with a greatest linear dimension equal to and above 250 μm can serve as an early stand-alone OCT biomarker for the future formation of GA.[123] What's more, the accurate detection of persistent hypertransmission defects on en face OCT images by graders demonstrates the feasibility of using this OCT biomarker to identify disease progression in eyes with nonexudative AMD.[124] The study of CC and GA is of great interest. It is already known that CC alterations in the area of GA and beyond the GA margin are based on histology findings. SS-OCTA was also able to detect the same finding.[19,125] The VISTA method suggested that the observed CC flow alterations in the border of GA and under nascent GA predominantly corresponded to flow impairment rather than complete CC atrophy.[126] Using SS-OCTA, the global CC FD was found to correlate with the enlargements rate of GA.[127] However, there is still no consistency regarding the visualization of CC in patients with GA, and whether they truly represent the absence of flow or merely reduced flow.[128] These findings still need to be further elucidated.

With SS-OCTA, different types of macular neovascularization (MNV) can be classified. Compared with SD-OCTA, SS-OCTA provides better visualization and more accurate quantification of MNV size with high repeatability across different scan patterns[129–131](Fig. 8). Using SS-OCTA, researchers discovered subclinical (also known as quiescent) type 1 and type 3 MNV.[132] In patients with intermediate AMD or GA secondary to nonexudative AMD in one eye and exudative AMD in the fellow eye, the risk of exudation was 15.2 times greater for eyes with subclinical MNV detected by SS-OCTA compared with eyes without subclinical MNV.[132] The 24-month risk of exudation was 13.6 times for

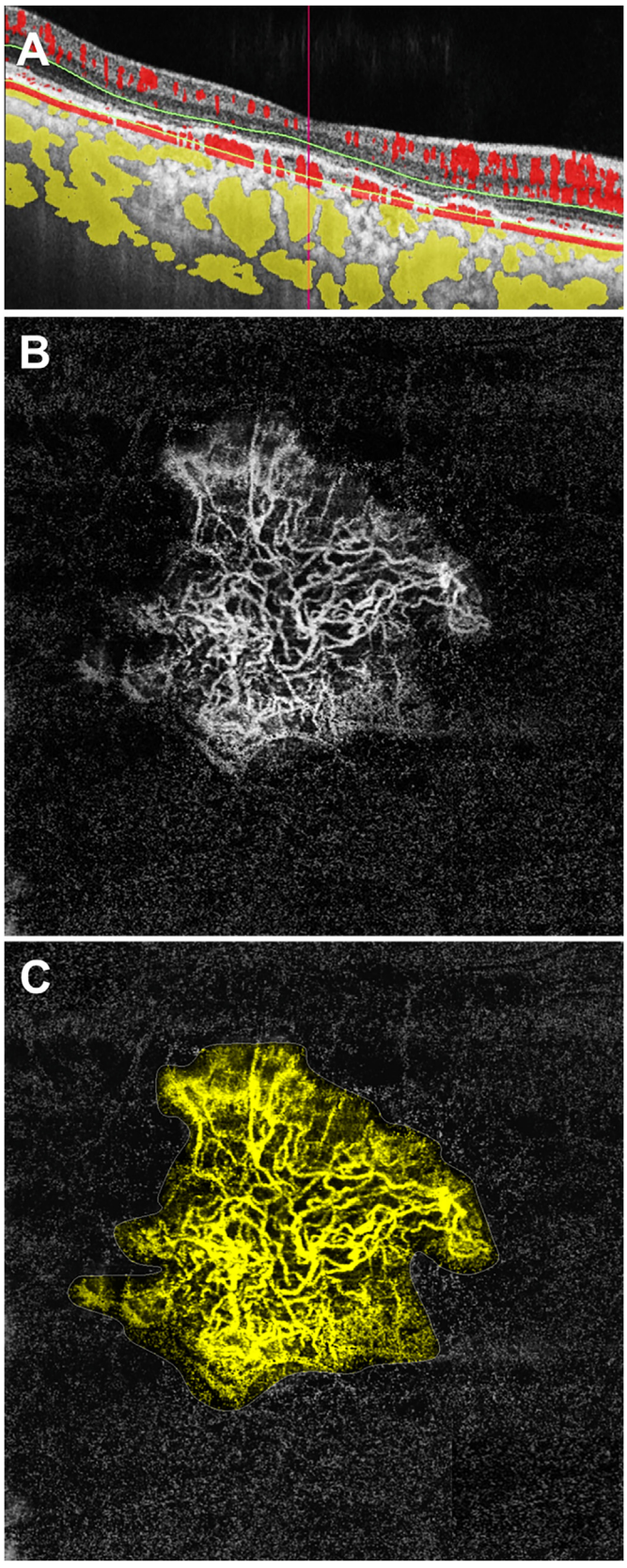

Fig. 8. The color-coded B-scan (A), outer retina slab (B) and automated flow area quantification (C) of an age-related macular degeneration patient with type 1 macular neovascularization using 6 × 6mm SS-OCTA (BM-400K BMizar, TowardPi Medical Technology, Beijing, China).

the same group of patients.[133] Using an automated algorithm, the size and vascularity of MNV can be measured, which helps evaluate the response of MNV to treatment.[134]

PCV is considered a subtype of neovascular AMD, which is more commonly observed in Asian populations. PCV is believed to represent a form of type 1 neovascularization associated with an abnormal branching vascular network (BVN) and aneurysmal dilations referred to as polyps.[135] Indocyanine green angiography (ICGA) is the current gold standard for PCV diagnosis.[136] Kim et al. performed SS-OCTA on 31 eyes of 30 patients with treatment-naïve PCV based on ICGA. They found that SS-OCTA was comparable to ICGA for the diagnosis of treatment-naïve PCV.[137] In addition, SS-OCTA might be better than ICGA in correctly identifying both polypoidal lesions and BVN in treatment-naïve PCV. Bo et al. noticed that previously described polypoidal lesions might appear as tangled vascular structures associated with BVN or type 2 MNV on SS-OCTA in eyes with PCV.[138] The same research group later found that the clusters of tangled vessels in PCV can evolve into typical type 1 MNV after anti-VEGF treatment.[139] For nonexudative PCV patients under treatment, both growth of BVN and progression of polypoidal lesions, including new appearance, enlargement, and reappearance of polypoidal lesions, were found to be characteristics associated with exudative recurrences.[140] Choroid is known to play an important role in the pathology of PCV. Focal or diffuse increases in CT, along with attenuation of the inner choroid, have also been widely documented by SS-OCT.[141] In treatment-naïve eyes with PCV, the decreases in pigment epithelial detachment (PED) volumes were correlated with the decrease in mean CT and the increase in CVI,[142] which provides a novel clue in the understanding of PCV.

5.6. SS-OCT and SS-OCTA for CSCR

SS-OCT provides great convenience in studying choroidal changes in CSCR. The en face SS-OCT images demonstrated that choroidal vascular areas were larger in the diseased and fellow eyes of CSCR patients than in age-matched normal controls.[143] According to a retrospective study, dilated vessels were seen at the level of Haller's layer in most cases of acute and chronic CSCR.[144] Interestingly, the vessels presented with focal dilation in eyes with acute CSCR, and the vessels presented with diffuse dilation in eyes with chronic CSCR. Above these dilated vessels at Haller's layer, attenuation of the inner choroidal layers was observed. Notably, all dilated choroidal vessels seen on en face SS-OCT images coincided with hyperpermeable lesions seen on the ICGA.

SS-OCTA also provides advantages when imaging eyes with chronic CSCR complicated by choroidal neovascularization (CNV).[145] In chronic CSCR, SS-OCTA had a sensitivity of 88% and a specificity of 100% to detect CNV, compared with conventional FA or ICGA.[146] In contrast, another study found that compared with OCTA, the FA was unable to characterize CNV in CSCR (with a very low sensitivity and moderate specificity), as none of the specific dye leakage patterns on FA correlated with CNV seen on OCTA, limiting its usefulness and accuracy in detecting CNV in these eyes.[147] When the overlapping of fluorescein leaking on FA influences the visualization of CNV, SS-OCTA is indispensable.[148] Xu's group also demonstrated the ability of SS-OCTA to qualitatively and quantitatively evaluate CNV in chronic CSCR complicated by flat irregular PED.[149] They found that half-dose PDT had favorable effects on chronic CSCR with CNV. Even though the mean area of CNV was larger at the 6-month follow-up, no signs of activity, such as subretinal fluid, were noticed. The authors suspected that the larger size of CNV after PDT might play a compensatory role in the macular. However, further research is required.

5.7. SS-OCT and SS-OCTA for MacTel2

MacTel2 is a primary neurodegenerative disease, with vascular changes limited to the macular. Therefore, SD-OCTA is sufficient for the diagnosis and monitoring MacTel2.[150] To date, only one study on MacTel2 has been published using SS-OCTA. The authors not only described the temporal microvascular changes around fovea correlating with FA leakage, but also demonstrated the superior ability of SS-OCTA in detecting sub-retinal neovascularization in proliferative MacTel2 compared with FA.[151] Using SS-OCT, studies about choroid change in MacTel2 have been conducted. Kumar et al. found significantly thicker choroids in MacTel2 patients compared to age-matched and gender-matched controls.[152] However, they failed to consider AL, the main influencing factor of CT. After adjusting for age and AL, there were no statistically significant differences in CT, CVC, and CVD when comparing eyes with MacTel2 to controls.[153]

5.8. SS-OCT and SS-OCTA for high myopia

High myopia is defined as a refractive error exceeding −6.0 diopters and/or AL longer than 26 mm, with characteristic degenerative changes in the sclera, retina, optic nerve, Bruch's membrane, RPE and choroid.[154] The larger FOV and deeper scanning window overcome the difficulty of imaging the posterior pole of the PM generated by the posterior staphyloma (Fig. 9). According to an observational cross-sectional study of 262 eyes of 139 pathologic myopia patients, SS-OCT was able to visualize the entire layer of the choroid and sclera.[155] By investigating the choroid and CC in anisomyopes using SS-OCT and SS-OCTA, Wu et al. found choroidal vascularity and CC blood perfusion were lower in the more myopic eyes of anisomyopic adults and these changes were correlated with the severity of myopia and choroidal thinning, suggesting that choroidal blood flow is disturbed in myopia eyes.[156] Wang's group found that ocular magnification significantly affects retinal vessels' quantification results and CC in myopic eyes.[157] They recommended correcting the magnification effect before quantifying the OCTA parameters in future studies. CNV is a common complication of myopia. Using SS-OCTA, the flow pattern and perforating vessels of CNV in myopia can be clearly delineated.[158]

5.9. SS-OCT and SS-OCTA for posterior uveitis

SS-OCT and SS-OCTA have been used to evaluate the structural and vascular changes in many types of posterior uveitis. They can also serve as an important noninvasive tool in assessing treatment responses. In the acute phase of sympathetic ophthalmia, thicker choroid and increased CVI were noticed based on SS-OCT imaging.[159] By assessing structural CT change after systemic corticosteroid therapy in Vogt-Koyanagi-Harada (VKH), significantly increased CT in the area with pretreatment CT of less than 100 μm and significantly decreased CT in the area with pretreatment CT of more than 300 μm were noticed, indicating choroidal remodeling.[160] Inflammatory CNV (iCNV) is a common complication of posterior uveitis. The presence of leaking of conventional dye-based angiography makes the diagnosis of iCNV challenging. OCTA is a useful tool for differentiating iCNV from other inflammatory lesions with high sensitivity and specificity.[161] Subretinal hyperreflective material in quiescent posterior uveitis imaging by SS-OCT and SS-OCTA may act as a useful biomarker to monitor activity and response to therapy in eyes with iCNV.[162] SS-OCTA was able to show outer photoreceptor disruption and sparing of the CC in multiple evanescent white dot syndrome (MEWDS).[163] In another MEWDS patient complicated with an atypical inflammatory subfoveal PED, a focal area of attenuated CC was noticed under the PED on SS-OCTA images. With the development of an automated quantification algorithm for CC lesion size in posterior uveitis patients, the disease activity would be monitored objectively.[164] It should be noticed that both SS-OCT and SS-OCTA lack information about leakage. However, by comparing the SS-OCTA images and FA in retinal vasculitis patients, researchers found retinal vascular leakage/staining on FA corresponded to increased perivascular retinal thickness on SS-OCTA.[165] Further studies are required to confirm whether SS-OCTA may serve as a semiquantitative alternative to FA in diagnosing and monitoring the response to treatment in uveitis patients presenting with

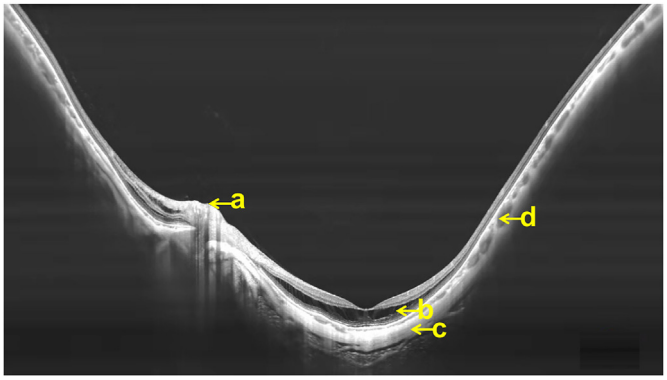

Fig. 9. A 24 mm SS-OCT B-scan of the left eye of a high myopia patient with posterior staphyloma and retinoschisis. (a) optic nerve, (b) retinoschisis in the macula, (c) sclera and (d) choroid. (BM-400K BMizar, TowardPi Medical Technology, Beijing, China).

retinal leakage or staining.

5.10. SS-OCT and SS-OCTA for optic nerve

SS-OCT is able to detect different aspects of the lamina cribrosa, including the anterior lamina cribrosa curvature, anterior lamina cribrosa depth, anterior lamina cribrosa insertions, laminar thickness, focal lamina cribrosa defects, and lamina cribrosa microarchitecture.[166] Compared with SD-OCT, SS-OCT did not show a higher detection rate of deep optic nerve structures. However, a larger area anterior surface of the lamina cribrosa was visible on SS-OCT.[167] In contrast, SS-OCT enabled calculation of optic nerve head drusen volume for all eyes, compared with SD-OCT fully visualizing the anterior and posterior drusen borders of no patient.[168] Using 3D-reconstructions and co-registered high--definition en face images extracted from a single densely sampled SS-OCT dataset, different patterns of optic disc pits were visualized in patients for the first time.[169] In preperimetric and early glaucoma, the retinal nerve fiber layer thickness map obtained from wide-field SS-OCT showed comparable sensitivity for distinguishing them from healthy eyes with conventional SD-OCT.[170]

6. Conclusions

The application of SS-OCT and SS-OCTA is not limited to this review. This system has been used in surgical retina area like macular hole, epiretinal membrane, and rhegmatogenous retinal detachment, as well as in investigating retina or choroid changes of systemic diseases. There is no doubt that this technology improves our understanding of ocular diseases and changes the clinical process. The data analysis function is built in most commercially available SS-OCT/SS-OCTA devices and keeps updating all the time. Together with new technology like artificial intelligence, new devices will continue to change our clinical practice.

Study approval

Not Applicable.

Author contributions

FZ, XD, and QZ wrote and revised the manuscript. JH, PY, and SL edited and revised the manuscript. PL, JZ, and XF supervised the whole manuscript drafting. All authors reviewed the results and approved the final version of the manuscript.

Funding

This research was supported by National Natural Youth Science Foundation Project of China (No. 82201196).

Declaration of competing interest

Jian Zhou is an employee of TowardPi (Beijing) Medical Technology Ltd, Shanghai, China. No conflicting relationship exists for other authors.

Acknowledgments

We thank Mingqian Zhu for the acquirement of all the images.

Abbreviations

SS-OCT	swept-source optical coherence tomography
SS-OCTA	swept-source optical coherence tomography angiography
FOV	field of view
FFT	Fast Fourier Transform
SNR	signal-to-noise ratio
VCSEL	vertical-cavity surface-emitting laser
ID-OCTA	inverse SNR and complex decorrelation OCTA
VISTA	variable interscan time analysis
ACA	anterior chamber angle
AL	axial length
IOL	intraocular lens
SBT	stromal bed thickness
ITC	iridotrabecular contact
PAS	peripheral anterior synechia
PPVPs	posterior precortical vitreous pockets
PVD	posterior vitreous detachment
DR	diabetic retinopathy
ROV/RAO	retinal artery/vein occlusion
AMD	age-related macular degeneration
PCV	polypoidal choroidal vasculopathy
CSCR	central serous chorioretinopathy
MacTel2	macular telangiectasia type 2
FAZ	fovea avascular zone
VDs	vasculature densities
CT	choroidal thickness
EDI	enhanced depth imaging
CVV	choroidal vessel volume
CSV	choroidal stroma volume
CVI	choroid vascularity index
CSVR	choroidal stroma-to-vessel volume ratio
CC	choriocapillaris
FDs	flow deficits
MAs	microaneurysms
NPAs	on-perfusion areas
IRMAs	intraretinal microvascular abnormalities
NV	neovascularization
UWF	ultrawide-field
RPD	reticular peseudodrusen
RPE	retinal pigment epithelium
GA	geographic atrophy
MNV	macular neovascularization
BVN	branching vascular network
ICGA	Indocyanine green angiography
CNV	choroidal neovascularization
PED	pigment epithelial detachment

References

1. Huang D, Swanson EA, Lin CP, et al. Optical coherence tomography. *Science*. 1991; 254(5035):1178–1181. https://doi.org/10.1126/science.1957169.
2. White B, Pierce M, Nassif N, et al. In vivo dynamic human retinal blood flow imaging using ultra-high-speed spectral domain optical coherence tomography. *Opt Express*. 2003;11(25):3490–3497. https://doi.org/10.1364/oe.11.003490.
3. Potsaid B, Baumann B, Huang D, et al. Ultrahigh speed 1050nm swept source/ Fourier domain OCT retinal and anterior segment imaging at 100,000 to 400,000 axial scans per second. *Opt Express*. 2010;18(19):20029–20048. https://doi.org/10.1364/OE.18.020029.
4. Leitgeb R, Hitzenberger C, Fercher A. Performance of fourier domain vs. time domain optical coherence tomography. *Opt Express*. 2003;11(8):889–894. https://doi.org/10.1364/oe.11.000889.
5. de Boer JF, Cense B, Park BH, et al. Improved signal-to-noise ratio in spectral-domain compared with time-domain optical coherence tomography. *Opt Lett*. 2003; 28(21):2067–2069. https://doi.org/10.1364/ol.28.002067.
6. Wojtkowski M. High-speed optical coherence tomography: basics and applications. *Appl Opt*. 2010;49(16):D30–D61. https://doi.org/10.1364/AO.49.000D30.
7. Kim TS, Joo J, Shin I, et al. 9.4 MHz A-line rate optical coherence tomography at 1300 nm using a wavelength-swept laser based on stretched-pulse active mode-locking. *Sci Rep*. 2020;10(1):9328. https://doi.org/10.1038/s41598-020-66322-0.
8. Lu CD, Waheed NK, Witkin A, et al. Microscope-integrated intraoperative ultrahigh-speed swept-source optical coherence tomography for widefield retinal and anterior segment imaging. *Ophthalmic Surg Lasers Imaging Retina*. 2018;49(2): 94–102. https://doi.org/10.3928/23258160-20180129-03.
9. Li P, Cheng Y, Li P, et al. Hybrid averaging offers high-flow contrast by cost apportionment among imaging time, axial, and lateral resolution in optical coherence tomography angiography. *Opt Lett*. 2016;41(17):3944–3947. https://doi.org/10.1364/OL.41.003944.
10. Cheng Y, Guo L, Pan C, et al. Statistical analysis of motion contrast in optical coherence tomography angiography. *J Biomed Opt*. 2015;20(11), 116004. https://doi.org/10.1117/1.JBO.20.11.116004.
11. Choi WJ, Reif R, Yousefi S, et al. Improved microcirculation imaging of human skin in vivo using optical microangiography with a correlation mapping mask. *J Biomed Opt*. 2014;19(3), 36010. https://doi.org/10.1117/1.JBO.19.3.036010.
12. Jia Y, Tan O, Tokayer J, et al. Split-spectrum amplitude-decorrelation angiography with optical coherence tomography. *Opt Express*. 2012;20(4):4710–4725. https://doi.org/10.1364/OE.20.004710.
13. Enfield J, Jonathan E, Leahy M. In vivo imaging of the microcirculation of the volar forearm using correlation mapping optical coherence tomography (cmOCT). *Biomed Opt Express*. 2011;2(5):1184–1193. https://doi.org/10.1364/BOE.2.001184.
14. Huang L, Fu Y, Chen R, et al. SNR-adaptive OCT angiography enabled by statistical characterization of intensity and decorrelation with multi-variate time series model. *IEEE Trans Med Imag*. 2019;38(11):2695–2704. https://doi.org/10.1109/TMI.2019.2910871.
15. Li H, Liu K, Cao T, et al. High performance OCTA enabled by combining features of shape, intensity, and complex decorrelation. *Opt Lett*. 2021;46(2):368–371. https://doi.org/10.1364/OL.405751.
16. Liu K, Zhu T, Yao L, et al. Noninvasive OCT angiography-based blood attenuation measurements correlate with blood glucose level in the mouse retina. *Biomed Opt Express*. 2021;12(8):4680–4688. https://doi.org/10.1364/BOE.430104.
17. Zhang Y, Li H, Cao T, et al. Automatic 3D adaptive vessel segmentation based on linear relationship between intensity and complex-decorrelation in optical coherence tomography angiography. *Quant Imag Med Surg*. 2021;11(3):895–906. https://doi.org/10.21037/qims-20-868.
18. Chen R, Yao L, Liu K, et al. Improvement of decorrelation-based OCT angiography by an adaptive spatial-temporal kernel in monitoring stimulus-evoked hemodynamic responses. *IEEE Trans Med Imag*. 2020;39(12):4286–4296. https://doi.org/10.1109/TMI.2020.3016334.
19. Choi W, Moult EM, Waheed NK, et al. Ultrahigh-speed, swept-source optical coherence tomography angiography in nonexudative age-related macular degeneration with geographic atrophy. *Ophthalmology*. 2015;122(12):2532–2544. https://doi.org/10.1016/j.ophtha.2015.08.029.
20. Wang RK, Zhang Q, Li Y, et al. Optical coherence tomography angiography-based capillary velocimetry. *J Biomed Opt*. 2017;22(6), 66008. https://doi.org/10.1117/1.JBO.22.6.066008.
21. Li Y, Wei W, Wang RK. Capillary flow homogenization during functional activation revealed by optical coherence tomography angiography based capillary velocimetry. *Sci Rep*. 2018;8(1):4107. https://doi.org/10.1038/s41598-018-22513-4.
22. Arriola-Villalobos P, Fernandez-Vigo JI, Diaz-Valle D, et al. Lower tear meniscus measurements using a new anterior segment swept-source optical coherence tomography and agreement with fourier-domain optical coherence tomography. *Cornea*. 2017;36(2):183–188. https://doi.org/10.1097/ICO.0000000000001086.
23. Fukuda R, Usui T, Miyai T, et al. Tear meniscus evaluation by anterior segment swept-source optical coherence tomography. *Am J Ophthalmol*. 2013;155(4): 620–624. https://doi.org/10.1016/j.ajo.2012.11.009, 624 e621-622.
24. Bolek B, Wylegala A, Teper S, et al. Treatment of conjunctival papilloma with topical interferon alpha-2b - case report. *Medicine (Baltim)*. 2020;99(7), e19181. https://doi.org/10.1097/MD.0000000000019181.
25. Dembski M, Nowinska A, Ulfik-Dembska K, et al. Swept source optical coherence tomography analysis of the selected eye's anterior segment parameters. *J Clin Med*. 2021;10(5). https://doi.org/10.3390/jcm10051094.
26. Han JY, Lee DC, Lee SY. Horizontal extraocular muscle and scleral anatomy in children: a swept-source anterior segment optical coherence tomography study. *Kor J Ophthalmol*. 2018;32(2):83–88. https://doi.org/10.3341/kjo.2017.0034.
27. Invernizzi A, Marchi S, Aldigeri R, et al. Objective quantification of anterior chamber inflammation: measuring cells and flare by anterior segment optical coherence tomography. *Ophthalmology*. 2017;124(11):1670–1677. https://doi.org/10.1016/j.ophtha.2017.05.013.
28. Kumar M, Shetty R, Jayadev C, et al. Comparability and repeatability of pachymetry in keratoconus using four noncontact techniques. *Indian J Ophthalmol*. 2015;63(9): 722–727. https://doi.org/10.4103/0301-4738.170987.
29. Steinberg J, Casagrande MK, Frings A, et al. Screening for subclinical keratoconus using swept-source fourier domain anterior segment optical coherence tomography. *Cornea*. 2015;34(11):1413–1419. https://doi.org/10.1097/ICO.0000000000000568.
30. Esaka Y, Kojima T, Dogru M, et al. Prediction of best-corrected visual acuity with swept-source optical coherence tomography parameters in keratoconus. *Cornea*. 2019;38(9):1154–1160. https://doi.org/10.1097/ICO.0000000000002043.
31. Szalai E, Nemeth G, Hassan Z, et al. Noncontact evaluation of corneal grafts: swept-source fourier domain OCT versus high-resolution Scheimpflug imaging. *Cornea*. 2017;36(4):434–439. https://doi.org/10.1097/ICO.0000000000001133.
32. Arnalich-Montiel F, Ortiz-Toquero S, Auladell C, et al. Accuracy of corneal thickness by swept-source optical coherence tomography and Scheimpflug camera in virgin and treated Fuchs endothelial dystrophy. *Cornea*. 2018;37(6):727–733. https://doi.org/10.1097/ICO.0000000000001530.
33. Satue M, Idoipe M, Sanchez-Perez A, et al. Evaluation of early graft detachment after Descemet membrane endothelial keratoplasty using new swept-source optical coherence tomography. *Cornea*. 2016;35(10):1279–1284. https://doi.org/10.1097/ICO.0000000000000925.
34. Ye C, Yu M, Jhanji V. Stromal bed thickness measurement during laser in situ keratomileusis using intraoperative optical coherence tomography. *Cornea*. 2015; 34(4):387–391. https://doi.org/10.1097/ICO.0000000000000345.
35. Georgeon C, Marciano I, Cuyaubere R, et al. Corneal and epithelial thickness mapping: comparison of swept-source- and spectral-domain-optical coherence tomography. *J Ophthalmol*. 2021;2021, 3444083. https://doi.org/10.1155/2021/3444083.
36. Gupta A, Ruminski D, Jimenez Villar A, et al. In vivo SS-OCT imaging of crystalline lens sutures. *Biomed Opt Express*. 2020;11(10):5388–5400. https://doi.org/10.1364/BOE.401254.
37. Li Z, Zhu Z, Li X, et al. Age-related changes in crystalline lens tilt and decentration: swept-source OCT study. *J Cataract Refract Surg*. 2021;47(10):1290–1295. https://doi.org/10.1097/j.jcrs.0000000000000632.
38. de Castro A, Benito A, Manzanera S, et al. Three-dimensional cataract crystalline lens imaging with swept-source optical coherence tomography. *Invest Ophthalmol Vis Sci*. 2018;59(2):897–903. https://doi.org/10.1167/iovs.17-23596.
39. Bras JEG, Sickenberger W, Hirnschall N, et al. Cataract quantification using swept-source optical coherence tomography. *J Cataract Refract Surg*. 2018;44(12): 1478–1481. https://doi.org/10.1016/j.jcrs.2018.08.009.
40. Hirnschall N, Buehren T, Bajramovic F, et al. Prediction of postoperative intraocular lens tilt using swept-source optical coherence tomography. *J Cataract Refract Surg*. 2017;43(6):732–736. https://doi.org/10.1016/j.jcrs.2017.01.026.
41. Lu Q, He W, Qian D, et al. Measurement of crystalline lens tilt in high myopic eyes before cataract surgery using swept-source optical coherence tomography. *Eye Vis (Lond)*. 2020;7:14. https://doi.org/10.1186/s40662-020-00176-5.
42. Tu R, Yu J, Savini G, et al. Agreement between two optical biometers based on large coherence length SS-OCT and Scheimpflug imaging/partial coherence interferometry. *J Refract Surg*. 2020;36(7):459–465. https://doi.org/10.3928/1081597X-20200420-02.
43. Grulkowski I, Liu JJ, Zhang JY, et al. Reproducibility of a long-range swept-source optical coherence tomography ocular biometry system and comparison with clinical biometers. *Ophthalmology*. 2013;120(11):2184–2190. https://doi.org/10.1016/j.ophtha.2013.04.007.
44. Qiao Y, Tan C, Zhang M, et al. Comparison of spectral domain and swept source optical coherence tomography for angle assessment of Chinese elderly subjects. *BMC Ophthalmol*. 2019;19(1):142. https://doi.org/10.1186/s12886-019-1145-7.
45. Huang W, Li X, Gao X, et al. The anterior and posterior biometric characteristics in primary angle-closure disease: data based on anterior segment optical coherence tomography and swept-source optical coherence tomography. *Indian J Ophthalmol*. 2021;69(4):865–870. https://doi.org/10.4103/ijo.IJO_936_20.
46. Pujari A, Yadav S, Sharma N, et al. Study 1: evaluation of the signs of deficient posterior capsule in posterior polar cataracts using anterior segment optical coherence tomography. *J Cataract Refract Surg*. 2020;46(9):1260–1265. https://doi.org/10.1097/j.jcrs.0000000000000246.
47. Porporato N, Baskaran M, Tun TA, et al. Assessment of circumferential angle closure with swept-source optical coherence tomography: a community based study. *Am J Ophthalmol*. 2019;199:133–139. https://doi.org/10.1016/j.ajo.2018.11.015.
48. Baskaran M, Ho SW, Tun TA, et al. Assessment of circumferential angle-closure by the iris-trabecular contact index with swept-source optical coherence tomography. *Ophthalmology*. 2013;120(11):2226–2231. https://doi.org/10.1016/j.ophtha.2013.04.020.
49. Foster PJ, Devereux JG, Alsbirk PH, et al. Detection of gonioscopically occludable angles and primary angle closure glaucoma by estimation of limbal chamber depth in Asians: modified grading scheme. *Br J Ophthalmol*. 2000;84(2):186–192. https://doi.org/10.1136/bjo.84.2.186.

50. Lavanya R, Wong TY, Friedman DS, et al. Determinants of angle closure in older Singaporeans. *Arch Ophthalmol*. 2008;126(5):686–691. https://doi.org/10.1001/archopht.126.5.686.
51. Nongpiur ME, Sakata LM, Friedman DS, et al. Novel association of smaller anterior chamber width with angle closure in Singaporeans. *Ophthalmology*. 2010;117(10):1967–1973. https://doi.org/10.1016/j.ophtha.2010.02.007.
52. Li X, Wang W, Huang W, et al. Difference of uveal parameters between the acute primary angle closure eyes and the fellow eyes. *Eye*. 2018;32(7):1174–1182. https://doi.org/10.1038/s41433-018-0056-9.
53. Nongpiur ME, He M, Amerasinghe N, et al. Lens vault, thickness, and position in Chinese subjects with angle closure. *Ophthalmology*. 2011;118(3):474–479. https://doi.org/10.1016/j.ophtha.2010.07.025.
54. Pekmezci M, Porco TC, Lin SC. Anterior segment optical coherence tomography as a screening tool for the assessment of the anterior segment angle. *Ophthalmic Surg Laser Imag*. 2009;40(4):389–398. https://doi.org/10.3928/15428877-20096030-07.
55. Sakata LM, Lavanya R, Friedman DS, et al. Comparison of gonioscopy and anterior segment ocular coherence tomography in detecting angle closure in different quadrants of the anterior chamber angle. *Ophthalmology*. 2008;115(5):769–774. https://doi.org/10.1016/j.ophtha.2007.06.030.
56. Porporato N, Baskaran M, Tun TA, et al. Understanding diagnostic disagreement in angle closure assessment between anterior segment optical coherence tomography and gonioscopy. *Br J Ophthalmol*. 2020;104(6):795–799. https://doi.org/10.1136/bjophthalmol-2019-314672.
57. Baskaran M, Iyer JV, Narayanaswamy AK, et al. Anterior segment imaging predicts incident gonioscopic angle closure. *Ophthalmology*. 2015;122(12):2380–2384. https://doi.org/10.1016/j.ophtha.2015.07.030.
58. Lai I, Mak H, Lai G, et al. Anterior chamber angle imaging with swept-source optical coherence tomography: measuring peripheral anterior synechia in glaucoma. *Ophthalmology*. 2013;120(6):1144–1149. https://doi.org/10.1016/j.ophtha.2012.12.006.
59. Dai Y, Zhang S, Shen M, et al. Identification of peripheral anterior synechia with anterior segment optical coherence tomography. *Graefes Arch Clin Exp Ophthalmol*. 2021;259(9):2753–2759. https://doi.org/10.1007/s00417-021-05220-1.
60. Loo Y, Tun TA, Vithana EN, et al. Association of peripheral anterior synechiae with anterior segment parameters in eyes with primary angle closure glaucoma. *Sci Rep*. 2021;11(1), 13906. https://doi.org/10.1038/s41598-021-93293-7.
61. Tun TA, Baskaran M, Perera SA, et al. Swept-source optical coherence tomography assessment of iris-trabecular contact after phacoemulsification with or without goniosynechialysis in eyes with primary angle closure glaucoma. *Br J Ophthalmol*. 2015;99(7):927–931. https://doi.org/10.1136/bjophthalmol-2014-306223.
62. Roberts PK, Goldstein DA, Fawzi AA. Anterior segment optical coherence tomography angiography for identification of Iris vasculature and staging of Iris neovascularization: a pilot study. *Curr Eye Res*. 2017;42(8):1136–1142. https://doi.org/10.1080/02713683.2017.1293113.
63. Skalet AH, Li Y, Lu CD, et al. Optical coherence tomography angiography characteristics of Iris melanocytic tumors. *Ophthalmology*. 2017;124(2):197–204. https://doi.org/10.1016/j.ophtha.2016.10.003.
64. Ang M, Devarajan K, Tan AC, et al. Anterior segment optical coherence tomography angiography for iris vasculature in pigmented eyes. *Br J Ophthalmol*. 2021;105(7):929–934. https://doi.org/10.1136/bjophthalmol-2020-316930.
65. Kose HC, Gunduz K, Hosal MB. Iris cysts: clinical features, imaging findings, and treatment results. *Turk J Ophthalmol*. 2020;50(1):31–36. https://doi.org/10.4274/tjo.galenos.2019.20633.
66. D'Aloisio R, Viggiano P, Borrelli E, et al. Changes in Iris perfusion following scleral buckle surgery for rhegmatogenous retinal detachment: an anterior segment optical coherence tomography angiography (AS-OCTA) study. *J Clin Med*. 2020;9(4). https://doi.org/10.3390/jcm9041231.
67. Liu JJ, Witkin AJ, Adhi M, et al. Enhanced vitreous imaging in healthy eyes using swept source optical coherence tomography. *PLoS One*. 2014;9(7), e102950. https://doi.org/10.1371/journal.pone.0102950.
68. Itakura H, Kishi S, Li D, et al. Observation of posterior precortical vitreous pocket using swept-source optical coherence tomography. *Invest Ophthalmol Vis Sci*. 2013;54(5):3102–3107. https://doi.org/10.1167/iovs.13-11769.
69. Li D, Kishi S, Itakura H, et al. Posterior precortical vitreous pockets and connecting channels in children on swept-source optical coherence tomography. *Invest Ophthalmol Vis Sci*. 2014;55(4):2412–2416. https://doi.org/10.1167/iovs.14-13967.
70. Leong BCS, Fragiotta S, Kaden TR, et al. OCT en face analysis of the posterior vitreous reveals topographic relationships among premacular bursa, prevascular fissures, and cisterns. *Ophthalmol Retina*. 2020;4(1):84–89. https://doi.org/10.1016/j.oret.2019.09.002.
71. Itakura H, Kishi S, Li D, et al. Vitreous changes in high myopia observed by swept-source optical coherence tomography. *Invest Ophthalmol Vis Sci*. 2014;55(3):1447–1452. https://doi.org/10.1167/iovs.13-13496.
72. Wang MD, Truong C, Mammo Z, et al. Swept source optical coherence tomography compared to ultrasound and biomicroscopy for diagnosis of posterior vitreous detachment. *Clin Ophthalmol*. 2021;15:507–512. https://doi.org/10.2147/OPTH.S297307.
73. Kraker JA, Kim JE, Koller EC, et al. Standard 6-mm compared with widefield 16.5-mm OCT for staging of posterior vitreous detachment. *Ophthalmol Retina*. 2020;4(11):1093–1102. https://doi.org/10.1016/j.oret.2020.05.006.
74. Tsukahara M, Mori K, Gehlbach PL, et al. Posterior vitreous detachment as observed by wide-angle OCT imaging. *Ophthalmology*. 2018;125(9):1372–1383. https://doi.org/10.1016/j.ophtha.2018.02.039.
75. Chiku Y, Hirano T, Takahashi Y, et al. Evaluating posterior vitreous detachment by widefield 23-mm swept-source optical coherence tomography imaging in healthy subjects. *Sci Rep*. 2021;11(1), 19754. https://doi.org/10.1038/s41598-021-99372-z.
76. Hayashi K, Sato T, Manabe SI, et al. Sex-related differences in the progression of posterior vitreous detachment with age. *Ophthalmol Retina*. 2019;3(3):237–243. https://doi.org/10.1016/j.oret.2018.10.017.
77. Xiong K, Gong X, Li W, et al. Comparison of macular thickness measurements using swept-source and spectral-domain optical coherence tomography in healthy and diabetic subjects. *Curr Eye Res*. 2021;46(10):1567–1573. https://doi.org/10.1080/02713683.2021.1908566.
78. Lee SY, Bae HW, Kwon HJ, et al. Repeatability and agreement of swept source and spectral domain optical coherence tomography evaluations of thickness sectors in normal eyes. *J Glaucoma*. 2017;26(2):e46–e53. https://doi.org/10.1097/IJG.0000000000000536.
79. Eastline M, Munk MR, Wolf S, et al. Repeatability of wide-field optical coherence tomography angiography in normal retina. *Transl Vis Sci Technol*. 2019;8(3):6. https://doi.org/10.1167/tvst.8.3.6.
80. Fang D, Tang FY, Huang H, et al. Repeatability, interocular correlation and agreement of quantitative swept-source optical coherence tomography angiography macular metrics in healthy subjects. *Br J Ophthalmol*. 2019;103(3):415–420. https://doi.org/10.1136/bjophthalmol-2018-311874.
81. Fernandez-Vigo JI, Kudsieh B, Shi H, et al. Normative database and determinants of macular vessel density measured by optical coherence tomography angiography. *Clin Exp Ophthalmol*. 2020;48(1):44–52. https://doi.org/10.1111/ceo.13648.
82. Kim K, You J, Park JR. Quantification of retinal microvascular parameters by severity of diabetic retinopathy using wide-field swept-source optical coherence tomography angiography. *Graefes Arch Clin Exp Ophthalmol*. 2021;259(8):2103–2111. https://doi.org/10.1007/s00417-021-05099-y.
83. Wen C, Pei C, Xu X, et al. Influence of axial length on parafoveal and peripapillary metrics from swept source optical coherence tomography angiography. *Curr Eye Res*. 2019;44(9):980–986. https://doi.org/10.1080/02713683.2019.1607393.
84. Fujiwara A, Morizane Y, Hosokawa M, et al. Factors affecting foveal avascular zone in healthy eyes: an examination using swept-source optical coherence tomography angiography. *PLoS One*. 2017;12(11), e0188572. https://doi.org/10.1371/journal.pone.0188572.
85. Wei WB, Xu L, Jonas JB, et al. Subfoveal choroidal thickness: the beijing eye study. *Ophthalmology*. 2013;120(1):175–180. https://doi.org/10.1016/j.ophtha.2012.07.048.
86. Ruiz-Medrano J, Flores-Moreno I, Pena-Garcia P, et al. Macular choroidal thickness profile in a healthy population measured by swept-source optical coherence tomography. *Invest Ophthalmol Vis Sci*. 2014;55(6):3532–3542. https://doi.org/10.1167/iovs.14-13868.
87. Hirata M, Tsujikawa A, Matsumoto A, et al. Macular choroidal thickness and volume in normal subjects measured by swept-source optical coherence tomography. *Invest Ophthalmol Vis Sci*. 2011;52(8):4971–4978. https://doi.org/10.1167/iovs.11-7729.
88. Touhami S, Philippakis E, Mrejen S, et al. Topographic variations of choroidal thickness in healthy eyes on swept-source optical coherence tomography. *Invest Ophthalmol Vis Sci*. 2020;61(3):38. https://doi.org/10.1167/iovs.61.3.38.
89. Lu J, Zhou H, Shi Y, et al. Interocular asymmetry of choroidal thickness and vascularity index measurements in normal eyes assessed by swept-source optical coherence tomography. *Quant Imag Med Surg*. 2022;12(1):781–795. https://doi.org/10.21037/qims-21-813.
90. Zhou H, Dai Y, Shi Y, et al. Age-related changes in choroidal thickness and the volume of vessels and stroma using swept-source OCT and fully automated algorithms. *Ophthalmol Retina*. 2020;4(2):204–215. https://doi.org/10.1016/j.oret.2019.09.012.
91. Zhang Q, Zheng F, Motulsky EH, et al. A novel strategy for quantifying choriocapillaris flow voids using swept-source OCT angiography. *Invest Ophthalmol Vis Sci*. 2018;59(1):203–211. https://doi.org/10.1167/iovs.17-22953.
92. Zhang Q, Shi Y, Zhou H, et al. Accurate estimation of choriocapillaris flow deficits beyond normal intercapillary spacing with swept source OCT angiography. *Quant Imag Med Surg*. 2018;8(7):658–666. https://doi.org/10.21037/qims.2018.08.10.
93. Zheng F, Zhang Q, Shi Y, et al. Age-dependent changes in the macular choriocapillaris of normal eyes imaged with swept-source optical coherence tomography angiography. *Am J Ophthalmol*. 2019;200:110–122. https://doi.org/10.1016/j.ajo.2018.12.025.
94. Sacconi R, Borrelli E, Corbelli E, et al. Quantitative changes in the ageing choriocapillaris as measured by swept source optical coherence tomography angiography. *Br J Ophthalmol*. 2019;103(9):1320–1326. https://doi.org/10.1136/bjophthalmol-2018-313004.
95. Nassisi M, Baghdasaryan E, Tepelus T, et al. Topographic distribution of choriocapillaris flow deficits in healthy eyes. *PLoS One*. 2018;13(11), e0207638. https://doi.org/10.1371/journal.pone.0207638.
96. Zhou K, Song S, Zhang Q, et al. Visualizing choriocapillaris using swept-source optical coherence tomography angiography with various probe beam sizes. *Biomed Opt Express*. 2019;10(6):2847–2860. https://doi.org/10.1364/BOE.10.002847.
97. Russell JF, Flynn Jr HW, Sridhar J, et al. Distribution of diabetic neovascularization on ultra-widefield fluorescein angiography and on simulated widefield OCT angiography. *Am J Ophthalmol*. 2019;207:110–120. https://doi.org/10.1016/j.ajo.2019.05.031.
98. Russell JF, Shi Y, Hinkle JW, et al. Longitudinal wide-field swept-source OCT angiography of neovascularization in proliferative diabetic retinopathy after panretinal photocoagulation. *Ophthalmol Retina*. 2019;3(4):350–361. https://doi.org/10.1016/j.oret.2018.11.008.

99. Russell JF, Shi Y, Scott NL, et al. Longitudinal angiographic evidence that intraretinal microvascular abnormalities can evolve into neovascularization. *Ophthalmol Retina*. 2020;4(12):1146–1150. https://doi.org/10.1016/j.oret.2020.06.010.
100. Cui Y, Zhu Y, Wang JC, et al. Comparison of widefield swept-source optical coherence tomography angiography with ultra-widefield colour fundus photography and fluorescein angiography for detection of lesions in diabetic retinopathy. *Br J Ophthalmol*. 2021;105(4):577–581. https://doi.org/10.1136/bjophthalmol-2020-316245.
101. Couturier A, Rey PA, Erginay A, et al. Widefield OCT-angiography and fluorescein angiography assessments of nonperfusion in diabetic retinopathy and edema treated with anti-vascular endothelial growth factor. *Ophthalmology*. 2019;126(12):1685–1694. https://doi.org/10.1016/j.ophtha.2019.06.022.
102. Salz DA, de Carlo TE, Adhi M, et al. Select features of diabetic retinopathy on swept-source optical coherence tomographic angiography compared with fluorescein angiography and normal eyes. *JAMA Ophthalmol*. 2016;134(6):644–650. https://doi.org/10.1001/jamaophthalmol.2016.0600.
103. La Mantia A, Kurt RA, Mejor S, et al. Comparing fundus fluorescein angiography and swept-source optical coherence tomography angiography in the evaluation of diabetic macular perfusion. *Retina*. 2019;39(5):926–937. https://doi.org/10.1097/IAE.0000000000002045.
104. Alibhai AY, De Pretto LR, Moult EM, et al. Quantification of retinal capillary nonperfusion in diabetics using wide-field optical coherence tomography angiography. *Retina*. 2020;40(3):412–420. https://doi.org/10.1097/IAE.0000000000002403.
105. Ryu G, Kim I, Sagong M. Topographic analysis of retinal and choroidal microvasculature according to diabetic retinopathy severity using optical coherence tomography angiography. *Graefes Arch Clin Exp Ophthalmol*. 2021;259(1):61–68. https://doi.org/10.1007/s00417-020-04785-7.
106. Cui Y, Zhu Y, Lu ES, et al. Widefield swept-source OCT angiography metrics associated with the development of diabetic vitreous hemorrhage: a prospective study. *Ophthalmology*. 2021;128(9):1312–1324. https://doi.org/10.1016/j.ophtha.2021.02.020.
107. Russell JF, Scott NL, Townsend JH, et al. Wide-field swept-source optical coherence tomography angiography of diabetic tractional retinal detachments before and after surgical repair. *Retina*. 2021;41(8):1587–1596. https://doi.org/10.1097/IAE.0000000000003146.
108. Arya M, Filho MB, Rebhun CB, et al. Analyzing relative flow speeds in diabetic retinopathy using variable interscan time analysis OCT angiography. *Ophthalmol Retina*. 2021;5(1):49–59. https://doi.org/10.1016/j.oret.2020.06.024.
109. Song P, Xu Y, Zha M, et al. Global epidemiology of retinal vein occlusion: a systematic review and meta-analysis of prevalence, incidence, and risk factors. *J Glob Health*. 2019;9(1), 010427. https://doi.org/10.7189/jogh.09.010427.
110. Sakimoto S, Gomi F, Sakaguchi H, et al. Analysis of retinal nonperfusion using depth-integrated optical coherence tomography images in eyes with branch retinal vein occlusion. *Invest Ophthalmol Vis Sci*. 2015;56(1):640–646. https://doi.org/10.1167/iovs.14-15673.
111. Imai A, Toriyama Y, Iesato Y, et al. En face swept-source optical coherence tomography detecting thinning of inner retinal layers as an indicator of capillary nonperfusion. *Eur J Ophthalmol*. 2015;25(2):153–158. https://doi.org/10.5301/ejo.5000514.
112. Moussa M, Leila M, Bessa AS, et al. Grading of macular perfusion in retinal vein occlusion using en-face swept-source optical coherence tomography angiography: a retrospective observational case series. *BMC Ophthalmol*. 2019;19(1):127. https://doi.org/10.1186/s12886-019-1134-x.
113. Kuehlewein L, An L, Durbin MK, et al. Imaging areas of retinal nonperfusion in ischemic branch retinal vein occlusion with swept-source OCT microangiography. *Ophthalmic Surg Lasers Imaging Retina*. 2015;46(2):249–252. https://doi.org/10.3928/23258160-20150213-19.
114. Kakihara S, Hirano T, Iesato Y, et al. Extended field imaging using swept-source optical coherence tomography angiography in retinal vein occlusion. *Jpn J Ophthalmol*. 2018;62(3):274–279. https://doi.org/10.1007/s10384-018-0590-9.
115. Shiraki A, Sakimoto S, Tsuboi K, et al. Evaluation of retinal nonperfusion in branch retinal vein occlusion using wide-field optical coherence tomography angiography. *Acta Ophthalmol*. 2019;97(6):e913–e918. https://doi.org/10.1111/aos.14087.
116. Costanzo E, Parravano M, Gilardi M, et al. Microvascular retinal and choroidal changes in retinal vein occlusion analyzed by two different optical coherence tomography angiography devices. *Ophthalmologica*. 2019;242(1):8–15. https://doi.org/10.1159/000496195.
117. Jiang X, Shen M, Wang L, et al. Validation of a novel automated algorithm to measure drusen volume and area using swept source optical coherence tomography angiography. *Transl Vis Sci Technol*. 2021;10(4):11. https://doi.org/10.1167/tvst.10.4.11.
118. Schaal KB, Legarreta AD, Feuer WJ, et al. Comparison between widefield en face swept-source OCT and conventional multimodal imaging for the detection of reticular pseudodrusen. *Ophthalmology*. 2017;124(2):205–214. https://doi.org/10.1016/j.ophtha.2016.10.009.
119. Liu J, Laiginhas R, Shen M, et al. Multimodal imaging and en face OCT detection of calcified drusen in eyes with age-related macular degeneration. *Ophthalmol Sci*. 2022;2(2). https://doi.org/10.1016/j.xops.2022.100162.
120. Sadda SR, Guymer R, Holz FG, et al. Consensus definition for atrophy associated with age-related macular degeneration on OCT: classification of atrophy report 3. *Ophthalmology*. 2018;125(4):537–548. https://doi.org/10.1016/j.ophtha.2017.09.028.
121. Guymer RH, Rosenfeld PJ, Curcio CA, et al. Incomplete retinal pigment epithelial and outer retinal atrophy in age-related macular degeneration: classification of atrophy meeting report 4. *Ophthalmology*. 2020;127(3):394–409. https://doi.org/10.1016/j.ophtha.2019.09.035.
122. Shi Y, Yang J, Feuer W, et al. Persistent hypertransmission defects on en face OCT imaging as a stand-alone precursor for the future formation of geographic atrophy. *Ophthalmol Retina*. 2021;5(12):1214–1225. https://doi.org/10.1016/j.oret.2021.02.004.
123. Laiginhas R, Shi Y, Shen M, et al. Persistent hypertransmission defects detected on en face swept source optical computed tomography images predict the formation of geographic atrophy in age-related macular degeneration. *Am J Ophthalmol*. 2022;237:58–70. https://doi.org/10.1016/j.ajo.2021.11.001.
124. Liu J, Laiginhas R, Corvi F, et al. Diagnosing persistent hypertransmission defects on en face OCT imaging of age-related macular degeneration. *Ophthalmol Retina*. 2022;6(5):387–397. https://doi.org/10.1016/j.oret.2022.01.011.
125. Nassisi M, Shi Y, Fan W, et al. Choriocapillaris impairment around the atrophic lesions in patients with geographic atrophy: a swept-source optical coherence tomography angiography study. *Br J Ophthalmol*. 2019;103(7):911–917. https://doi.org/10.1136/bjophthalmol-2018-312643.
126. Moult EM, Waheed NK, Novais EA, et al. Swept-source optical coherence tomography angiography reveals choriocapillaris alterations in eyes with nascent geographic atrophy and drusen-associated geographic atrophy. *Retina*. 2016;36(Suppl 1):S2–S11. https://doi.org/10.1097/IAE.0000000000001287.
127. Thulliez M, Zhang Q, Shi Y, et al. Correlations between choriocapillaris flow deficits around geographic atrophy and enlargement rates based on swept-source OCT imaging. *Ophthalmol Retina*. 2019;3(6):478–488. https://doi.org/10.1016/j.oret.2019.01.024.
128. Waheed NK, Moult EM, Fujimoto JG, et al. Optical coherence tomography angiography of dry age-related macular degeneration. *Dev Ophthalmol*. 2016;56:91–100. https://doi.org/10.1159/000442784.
129. Miller AR, Roisman L, Zhang Q, et al. Comparison between spectral-domain and swept-source optical coherence tomography angiographic imaging of choroidal neovascularization. *Invest Ophthalmol Vis Sci*. 2017;58(3):1499–1505. https://doi.org/10.1167/iovs.16-20969.
130. Novais EA, Adhi M, Moult EM, et al. Choroidal neovascularization analyzed on ultrahigh-speed swept-source optical coherence tomography angiography compared to spectral-domain optical coherence tomography angiography. *Am J Ophthalmol*. 2016;164:80–88. https://doi.org/10.1016/j.ajo.2016.01.011.
131. Zheng F, Zhang Q, Motulsky EH, et al. Comparison of neovascular lesion area measurements from different swept-source OCT angiographic scan patterns in age-related macular degeneration. *Invest Ophthalmol Vis Sci*. 2017;58(12):5098–5104. https://doi.org/10.1167/iovs.17-22506.
132. de Oliveira Dias JR, Zhang Q, Garcia JMB, et al. Natural history of subclinical neovascularization in nonexudative age-related macular degeneration using swept-source OCT angiography. *Ophthalmology*. 2018;125(2):255–266. https://doi.org/10.1016/j.ophtha.2017.08.030.
133. Yang J, Zhang Q, Motulsky EH, et al. Two-year risk of exudation in eyes with nonexudative age-related macular degeneration and subclinical neovascularization detected with swept source optical coherence tomography angiography. *Am J Ophthalmol*. 2019;208:1–11. https://doi.org/10.1016/j.ajo.2019.06.017.
134. Zhang Q, Zhang A, Lee CS, et al. Projection artifact removal improves visualization and quantitation of macular neovascularization imaged by optical coherence tomography angiography. *Ophthalmol Retina*. 2017;1(2):124–136. https://doi.org/10.1016/j.oret.2016.08.005.
135. Wong CW, Yanagi Y, Lee WK, et al. Age-related macular degeneration and polypoidal choroidal vasculopathy in Asians. *Prog Retin Eye Res*. 2016;53:107–139. https://doi.org/10.1016/j.preteyeres.2016.04.002.
136. Koh A, Lee WK, Chen LJ, et al. EVEREST study: efficacy and safety of verteporfin photodynamic therapy in combination with ranibizumab or alone versus ranibizumab monotherapy in patients with symptomatic macular polypoidal choroidal vasculopathy. *Retina*. 2012;32(8):1453–1464. https://doi.org/10.1097/IAE.0b013e31824f91e8.
137. Kim K, Yang J, Feuer W, et al. A comparison study of polypoidal choroidal vasculopathy imaged with indocyanine green angiography and swept-source optical coherence tomography angiography. *Am J Ophthalmol*. 2020;217:240–251. https://doi.org/10.1016/j.ajo.2020.05.017.
138. Bo Q, Yan Q, Shen M, et al. Appearance of polypoidal lesions in patients with polypoidal choroidal vasculopathy using swept-source optical coherence tomographic angiography. *JAMA Ophthalmol*. 2019;137(6):642–650. https://doi.org/10.1001/jamaophthalmol.2019.0449.
139. Shen M, Bo Q, Song M, et al. Replacement of polyps with type 1 macular neovascularization in polypoidal choroidal vasculopathy imaged with swept source OCT angiography. *Am J Ophthalmol Case Rep*. 2021;22, 101057. https://doi.org/10.1016/j.ajoc.2021.101057.
140. Bo Q, Zhang M, Chen J, et al. Progression of polypoidal lesions associated with exudative recurrence in polypoidal choroidal vasculopathy. *Ophthalmology*. 2022. https://doi.org/10.1016/j.ophtha.2022.09.013.
141. Dansingani KK, Balaratnasingam C, Naysan J, et al. En face imaging of pachychoroid spectrum disorders with swept-source optical coherence tomography. *Retina*. 2016;36(3):499–516. https://doi.org/10.1097/IAE.0000000000000742.
142. Shen M, Zhou H, Kim K, et al. Choroidal changes in eyes with polypoidal choroidal vasculopathy after anti-VEGF therapy imaged with swept-source OCT angiography. *Invest Ophthalmol Vis Sci*. 2021;62(15):5. https://doi.org/10.1167/iovs.62.15.5.
143. Kuroda Y, Ooto S, Yamashiro K, et al. Increased choroidal vascularity in central serous chorioretinopathy quantified using swept-source optical coherence tomography. *Am J Ophthalmol*. 2016;169:199–207. https://doi.org/10.1016/j.ajo.2016.06.043.

144. Lee WJ, Lee JW, Park SH, et al. En face choroidal vascular feature imaging in acute and chronic central serous chorioretinopathy using swept source optical coherence tomography. *Br J Ophthalmol*. 2017;101(5):580–586. https://doi.org/10.1136/bjophthalmol-2016-308428.
145. Sulzbacher F, Schutze C, Burgmuller M, et al. Clinical evaluation of neovascular and non-neovascular chronic central serous chorioretinopathy (CSC) diagnosed by swept source optical coherence tomography angiography (SS OCTA). *Graefes Arch Clin Exp Ophthalmol*. 2019;257(8):1581–1590. https://doi.org/10.1007/s00417-019-04297-z.
146. Stattin M, Ahmed D, Forster J, et al. Detection of secondary choroidal neovascularization in chronic central serous chorioretinopathy by swept source-optical coherence tomography angiography. *Acta Ophthalmol*. 2019;97(1):e135–e136. https://doi.org/10.1111/aos.13855.
147. Bansal R, Dogra M, Mulkutkar S, et al. Optical coherence tomography angiography versus fluorescein angiography in diagnosing choroidal neovascularization in chronic central serous chorioretinopathy. *Indian J Ophthalmol*. 2019;67(7):1095–1100. https://doi.org/10.4103/ijo.IJO_1238_18.
148. Moussa M, Leila M, Khalid H, et al. Detection of silent type I choroidal neovascular membrane in chronic central serous chorioretinopathy using en face swept-source optical coherence tomography angiography. *J Ophthalmol*. 2017;2017, 6913980. https://doi.org/10.1155/2017/6913980.
149. Guo J, Tang W, Xu S, et al. OCTA evaluation of treatment-naive flat irregular PED (FIPED)-associated CNV in chronic central serous chorioretinopathy before and after half-dose PDT. *Eye*. 2021;35(10):2871–2878. https://doi.org/10.1038/s41433-020-01345-5.
150. Zheng F, Motulsky EH, de Oliveira Dias JR, et al. OCT angiography helps distinguish between proliferative macular telangiectasia type 2 and neovascular age-related macular degeneration. *Ophthalmic Surg Lasers Imaging Retina*. 2018;49(5):303–312. https://doi.org/10.3928/23258160-20180501-03.
151. Thorell MR, Zhang Q, Huang Y, et al. Swept-source OCT angiography of macular telangiectasia type 2. *Ophthalmic Surg Lasers Imaging Retina*. 2014;45(5):369–380. https://doi.org/10.3928/23258160-20140909-06.
152. Kumar V, Kumawat D, Kumar P. Swept source optical coherence tomography analysis of choroidal thickness in macular telangiectasia type 2: a case-control study. *Graefes Arch Clin Exp Ophthalmol*. 2019;257(3):567–573. https://doi.org/10.1007/s00417-018-04215-9.
153. Wang JC, Lains I, Oellers P, et al. Choroidal thickness and vascular density in macular telangiectasia type 2 using en face swept-source optical coherence tomography. *Br J Ophthalmol*. 2019;103(11):1584–1589. https://doi.org/10.1136/bjophthalmol-2018-313414.
154. Ruiz-Medrano J, Montero JA, Flores-Moreno I, et al. Myopic maculopathy: current status and proposal for a new classification and grading system (ATN). *Prog Retin Eye Res*. 2019;69:80–115. https://doi.org/10.1016/j.preteyeres.2018.10.005.
155. Meng LH, Yuan MZ, Zhao XY, et al. Wide-field swept source optical coherence tomography evaluation of posterior segment changes in highly myopic eyes. *Eur J Ophthalmol*. 2021, 11206721211062362. https://doi.org/10.1177/11206721211062362.
156. Wu H, Zhang G, Shen M, et al. Assessment of choroidal vascularity and choriocapillaris blood perfusion in anisomyopic adults by SS-OCT/OCTA. *Invest Ophthalmol Vis Sci*. 2021;62(1):8. https://doi.org/10.1167/iovs.62.1.8.
157. Dai Y, Xin C, Zhang Q, et al. Impact of ocular magnification on retinal and choriocapillaris blood flow quantification in myopia with swept-source optical coherence tomography angiography. *Quant Imag Med Surg*. 2021;11(3):948–956. https://doi.org/10.21037/qims-20-1011.
158. Sayanagi K, Hara C, Fukushima Y, et al. Flow pattern and perforating vessels in three different phases of myopic choroidal neovascularization seen by swept-source optical coherence tomography angiography. *Graefes Arch Clin Exp Ophthalmol*. 2021;259(9):2615–2624. https://doi.org/10.1007/s00417-021-05134-y.
159. Agrawal R, Jain M, Khan R, et al. Choroidal structural changes in sympathetic ophthalmia on swept-source optical coherence tomography. *Ocul Immunol Inflamm*. 2021;29(3):537–542. https://doi.org/10.1080/09273948.2019.1685110.
160. Jaisankar D, Raman R, Sharma HR, et al. Choroidal and retinal anatomical responses following systemic corticosteroid therapy in vogt-koyanagi-harada disease using swept-source optical coherence tomography. *Ocul Immunol Inflamm*. 2019;27(2):235–243. https://doi.org/10.1080/09273948.2017.1332231.
161. Aggarwal K, Agarwal A, Sharma A, et al. Detection of type 1 choroidal neovascular membranes using optical coherence tomography angiography in tubercular posterior uveitis. *Retina*. 2019;39(8):1595–1606. https://doi.org/10.1097/IAE.0000000000002176.
162. Arora A, Agarwal A, Bansal R, et al. Subretinal Hyperreflective Material (SHRM) as biomarker of activity in Exudative and Non- exudative inflammatory choroidal neovascularization. *Ocul Immunol Inflamm*. 2021:1–8. https://doi.org/10.1080/09273948.2021.1980813.
163. Yannuzzi NA, Swaminathan SS, Zheng F, et al. Swept-source OCT angiography shows sparing of the choriocapillaris in multiple evanescent white dot syndrome. *Ophthalmic Surg Lasers Imaging Retina*. 2017;48(1):69–74. https://doi.org/10.3928/23258160-20161219-10.
164. Swaminathan SS, Zheng F, Miller AR, et al. Swept-source OCT angiography of multiple evanescent white dot syndrome with inflammatory retinal pigment epithelial detachment. *Ophthalmic Surg Lasers Imaging Retina*. 2018;49(2):145–151. https://doi.org/10.3928/23258160-20180129-12.
165. Noori J, Shi Y, Yang J, et al. A novel method to detect and monitor retinal vasculitis using swept-source OCT angiography. *Ophthalmol Retina*. 2021;5(12):1226–1234. https://doi.org/10.1016/j.oret.2021.02.007.
166. Takusagawa HL, Hoguet A, Junk AK, et al. Swept-source OCT for evaluating the lamina cribrosa: a report by the American academy of ophthalmology. *Ophthalmology*. 2019;126(9):1315–1323. https://doi.org/10.1016/j.ophtha.2019.03.044.
167. Loureiro MM, Vianna JR, Danthurebandara VM, et al. Visibility of optic nerve head structures with spectral-domain and swept-source optical coherence tomography. *J Glaucoma*. 2017;26(9):792–797. https://doi.org/10.1097/IJG.0000000000000740.
168. Tsikata E, Verticchio Vercellin AC, Falkenstein I, et al. Volumetric measurement of optic nerve head drusen using swept-source optical coherence tomography. *J Glaucoma*. 2017;26(9):798–804. https://doi.org/10.1097/IJG.0000000000000707.
169. Maertz J, Kolb JP, Klein T, et al. Combined in-depth, 3D, en face imaging of the optic disc, optic disc pits and optic disc pit maculopathy using swept-source megahertz OCT at 1050 nm. *Graefes Arch Clin Exp Ophthalmol*. 2018;256(2):289–298. https://doi.org/10.1007/s00417-017-3857-9.
170. Lee WJ, Oh S, Kim YK, et al. Comparison of glaucoma-diagnostic ability between wide-field swept-source OCT retinal nerve fiber layer maps and spectral-domain OCT. *Eye*. 2018;32(9):1483–1492. https://doi.org/10.1038/s41433-018-0104-5.